Mapping reactor neutrino spectra from TAO to JUNO

Francesco Capozzi,[1] Eligio Lisi,[2] and Antonio Marrone[3,2]
[1]*Max-Planck-Institut für Physik (Werner-Heisenberg-Institut), Föhringer Ring 6, 80805 München, Germany*
[2]*Istituto Nazionale di Fisica Nucleare, Sezione di Bari, Via Orabona 4, 70126 Bari, Italy*
[3]*Dipartimento Interateneo di Fisica "Michelangelo Merlin," Via Amendola 173, 70126 Bari, Italy*

(Received 6 June 2020; accepted 20 July 2020; published 2 September 2020)

The Jiangmen Underground Neutrino Observatory (JUNO) project aims at probing, at the same time, the two main frequencies of three-flavor neutrino oscillations, as well as their interference related to the mass ordering (normal or inverted), at a distance of ∼53 km from two powerful reactor complexes in China, at Yangjiang and Taishan. In the latter complex, the unoscillated spectrum from one reactor core is planned to be closely monitored by the Taishan Antineutrino Observatory (TAO), expected to have better resolution ($\times 1/2$) and higher statistics ($\times 30$) than JUNO. In the context of ν energy spectra endowed with fine-structure features from summation calculations, we analyze in detail the effects of energy resolution and nucleon recoil on observable event spectra. We show that a model spectrum in TAO can be mapped into a corresponding spectrum in JUNO through appropriate convolutions. The mapping is exact in the hypothetical case without oscillations and holds to a very good accuracy in the real case with oscillations. We then analyze the sensitivity to mass ordering of JUNO (and its precision oscillometry capabilities) assuming a single reference spectrum, as well as bundles of variant spectra, as obtained by changing nuclear input uncertainties in summation calculations from a publicly available toolkit. We show through an χ^2 analysis that variant spectra induce little reduction of the sensitivity in JUNO, especially when TAO constraints are included. Subtle aspects of the statistical analysis of variant spectra are also discussed.

DOI: 10.1103/PhysRevD.102.056001

I. INTRODUCTION

Experiments based on electron antineutrinos ($\bar{\nu}_e$) from nuclear reactors—referred to as reactor neutrinos hereafter—have marked the history of neutrino physics [1–5]. In the neutrino oscillation era, they have been—and continue to be—a major tool for both discoveries and precision measurements [6–8]. In particular, reactor experiments at long baseline [9] and short baseline (SBL) [10–12] have observed the oscillation patterns governed by the mass-mixing parameters $(\Delta m^2_{21}, \theta_{12})$ and $(\Delta m^2_{32}, \theta_{13})$, respectively [13]. At medium baseline (MBL), reactor experiments with high statistics and resolution could observe both patterns and their interference, probing $\alpha = \mathrm{sign}(\Delta m^2_{32}/\Delta m^2_{21}) = \pm 1$ and thus the ν mass ordering, either "normal ordering" (NO, $\alpha = +1$) or "inverted ordering" (IO, $\alpha = -1$) [14]. In order to perform such MBL oscillation searches, as well as a wider physics program, the Jiangmen Underground Neutrino Observatory (JUNO) is being built near Kaiping (China), at equal baselines ($L \sim 53$ km) from the Taishan and Yangjiang reactor complexes [15,16].

In this context, the neutrino energy spectra at the reactor source(s) represent important inputs, that should be understood and computed with an accuracy comparable to the experimental one. Reactor neutrino spectra have usually been obtained either by conversion from measured electron spectra ("conversion" approach) or by summing over thousands of beta transitions tabulated in nuclear databases (*ab initio* or "summation" approach), and sometimes in combination ("hybrid" approach) [17,18]. In the last decade, these approaches have been challenged by new data (or by reanalyses of old data) that do not compare well with computed spectra, even invoking nonstandard physics such as sterile neutrinos [19–21] (not considered herein). A primary example is the unexpected "bump" observed around 5 MeV in current SBL oscillation experiments [10–12,22] (and possibly in older data [23]), whose understanding is still entangled with many issues, including normalization anomalies in the total flux and its fuel components [24–31], incomplete information in nuclear databases [32–35], possible energy-scale systematics [36], suppression of β-decay spectra systematics [37] via total absorption [38–43] and other techniques [44], and, on the

theory side, improved calculations of (allowed and forbidden) β decay spectra [45–53].

Another layer of complexity, pointed out in summation calculations of the neutrino energy spectrum, is the presence of sawtoothlike substructures, as expected from Coulomb effects in individual β decays [54–56]. These fine-structure features have not been observed within the resolution of current experiments, with the possible exception of a hint discussed in [57]. Observing or constraining (at least a few) prominent substructures in future, high-resolution and high-statistics reactor neutrino experiments, would be beneficial both for nuclear spectroscopy (allowing to pin down the spectral contributions of specific fission products [57]), and for neutrino oscillometry (reducing small-scale fuzzy uncertainties that might affect the JUNO sensitivity to mass ordering [58]). Although the latter benefit may be marginal if one assumes "known" substructures from nuclear databases [59,60], the observation of unexpected spectral anomalies at large energy scales (normalization and bump issues) provides a warning about the possible emergence of "unknown" features also at small scales. For a recent and comprehensive overview of current issues and future prospects in understanding reactor neutrino spectra, see the contributions in [61].

In oscillation searches at reactor experiments, spectral uncertainties can be efficiently suppressed by comparing near (unoscillated) and far (oscillated) event spectra [62,63], as performed in [10–12]. In the context of JUNO, a concept for a high-resolution near detector was mentioned in [64] and further detailed in [65,66]. This concept has evolved into a full-fledged project, the Taishan Antineutrino Observatory (TAO) [67–71].[1] TAO is expected to monitor the unoscillated spectrum emitted by one of the Taishan nuclear reactors, with a gain of about $\times 1/2$ in energy resolution and $\times 30$ in event statistics with respect to the oscillated spectrum at JUNO. Independently of neutrino oscillations, high-resolution spectral measurements at TAO will set unprecedented benchmarks [67] for research in nuclear fission physics [73–75] and for broader investigations of the neutrino-nuclear response in particle physics and astrophysics [76]. In general, progress in neutrino and nuclear physics, coupled with precision measurements at TAO, is expected to significantly constrain the range of neutrino spectral models to be used in future JUNO data analyses.

In this work, we build upon our previous studies of precision oscillometry [77,78], but considering summation spectra with substructures and possible uncertainties. We use the publicly available toolkit Oklo [79,80] to generate ensembles of spectra within quoted errors on yields, branching ratios, and end point energies for each decay. This toolkit, although currently not updated in terms of nuclear database inputs (taken as of 2015 [79]), is appropriate for our methodological purposes and numerical experiments. For simplicity, we shall assume that the underlying neutrino spectra are the same in TAO and JUNO. In reality, the former will closely monitor only one reactor core in Taishan, while the latter will detect a signal generated by several reactors in both Taishan and Yangjiang, with different fuel evolutions [67,72,81]. The related fuel corrections will require detailed information and modeling for each reactor, that are beyond the scope of this paper and will be studied elsewhere.

Our work can be divided in two main parts. In the first part (Secs. II and III), we discuss the formal relations between the TAO and JUNO energy spectra. We start by revisiting in detail the effects of resolution and recoil that, although well known in principle, are not always properly distinguished and implemented at the level of accuracy required by future measurements. Then, we show that any observable energy spectrum of events in TAO can be mapped into a corresponding spectrum in JUNO by a proper convolution. In particular, we show that this mapping can be exactly performed in the hypothetical case of no oscillations (Sec. II) and can be very accurately generalized, via an ansatz, to the real case of neutrino oscillations (Sec. III). These results allow to predict the JUNO spectrum directly from a model for the observable event spectrum at the TAO detector, rather than from a model for the unobservable neutrino spectrum at the reactor source.

In the second part of the paper, we perform quantitative studies of the mass-ordering sensitivity and precision oscillometry in JUNO, first by considering a single reference spectrum with substructures, and then by adding bundles of variant spectra to be constrained by TAO. In Sec. IV, we revisit our previous analysis [78] including the reference Oklo spectrum, new priors for the oscillation parameters, and reduced error bands for smooth flux-shape and energy-scale systematics. We confirm the accuracy of the mapping and discuss the impact of these new inputs. In Sec. V, we generate bundles of Oklo variants around the previous reference spectrum. We perform an χ^2 analysis of variant spectra in JUNO, alternative to the Fourier analysis in [59], and highlight several statistical issues arising from sampling the nuclear input uncertainties. By varying all the known nuclear data inputs, we generate and analyze an ensemble of 10^5 spectra in JUNO, but find no reduction of the sensitivity to mass ordering, with or without TAO; we trace this unexpected result to subtle undersampling issues in the generated bundle of spectra. We repeat the analysis by constructing an equally numerous but "more densely sampled" bundle and find a small reduction of the JUNO sensitivity, consistent with [59] and improved with the help of TAO. These results, based on "known" nuclear inputs, suggest some cautionary comments on parametrizations of

[1]While this paper was being written, the complete TAO conceptual design report (CDR) was released [72]. For the purposes of our work, the CDR confirms the basic characteristics of TAO that we have adopted from previous reports [67–71].

"unknown" substructure uncertainties, as those considered in [58]. We also analyze the JUNO accuracy on the relevant mass-mixing parameters, which is found to be basically unaffected by fine-structure issues. Our results are summarized in Sec. VI.

II. MAPPING THE SPECTRUM FROM TAO TO JUNO WITHOUT OSCILLATIONS

Reactor neutrinos can be detected through the inverse beta decay (IBD) process $\bar{\nu}_e + p \to e^+ + n$ followed by e^+ annihilation and delayed n capture. Using the notation of [77,78], we focus on the following two energy variables for IBD events:

$$E = \text{unobservable } \bar{\nu}_e \text{ energy}, \tag{1}$$

$$E_{\text{vis}} = \text{observable (visible) energy of the event}. \tag{2}$$

We also consider the unobservable neutrino spectrum S_ν, as given by the reactor ν flux $\Phi(E)$ times the IBD cross section [82,83] $\sigma_\nu(E)$,

$$S_\nu(E) = \Phi(E)\sigma_\nu(E), \tag{3}$$

and the observable IBD event spectrum at the detector X,

$$S_X = S_X(E_{\text{vis}}), \quad X = T, J, \tag{4}$$

where the subscripts T and J shall refer to TAO and JUNO, respectively.

In this section, we show that, for no oscillation, the TAO spectrum can be exactly mapped into the JUNO spectrum,

$$S_T(E_{\text{vis}}) \to S_J(E_{\text{vis}}), \tag{5}$$

without knowing *a priori* $S_\nu(E)$. This result is nontrivial in the presence of resolution and recoil effects, that we discuss below following [77]. The mapping will be extended to the oscillation case in Sec. III.

A. Detector resolution

In a detector with perfect energy resolution, E_{vis} would be equal to

$$E_{\text{vis}} = E_e + m_e \text{ (perfect resolution)}, \tag{6}$$

where E_e and m_e are the total e^+ energy and mass, respectively.

In reality, due to finite photon statistics and other instrumental effects, E_{vis} is distributed around $E_e + m_e$ according to a resolution function r_X,

$$r_X(E_{\text{vis}}, E_e + m_e|\sigma_X^2) = \frac{1}{\sqrt{2\pi\sigma_X^2}}\exp\left(-\frac{1}{2}\frac{(E_{\text{vis}} - E_e - m_e)^2}{\sigma_X^2}\right), \tag{7}$$

where σ_X^2 is the energy resolution variance for the detector X. For TAO, we adopt, as a representative value of σ_T [67–71],

$$\frac{\sigma_T}{E_{\text{vis}}} = \frac{1.7\%}{\sqrt{E_{\text{vis}}}}, \tag{8}$$

while for JUNO we take σ_J/E_{vis} as in [78] (roughly equal to $3\%/\sqrt{E_{\text{vis}}}$).

B. Nucleon recoil

If recoil effects were neglected in IBD events, $E_e + m_e$ would be related to E via

$$E_e + m_e = E - 0.783 \text{ MeV (no recoil)}. \tag{9}$$

Nucleon recoil induces an angle-dependent deficit in E_e, making this relation an upper bound. In general, E_e ranges between two kinematical extrema $E_{1,2}(E)$ [see Eqs. (12) and (13) in Ref. [83]],

$$E_1 \le E_e \le E_2 (< E - m_e - 0.783 \text{ MeV}), \tag{10}$$

with a relatively flat distribution (see [77] and Fig. 2 therein). As in [77,78], we approximate this distribution through a top-hat function,

$$t(E, E_e) = \frac{1}{\sigma_\nu(E)}\frac{d\sigma_\nu(E, E_e)}{dE_e} \simeq \begin{cases} (E_2 - E_1)^{-1} & \text{for } E_1 \le E_e \le E_2, \\ 0 & \text{otherwise}, \end{cases} \tag{11}$$

where $d\sigma_\nu/dE_e$ is the differential IBD cross section [83]. We have explicitly checked for TAO (as we did in [77] for JUNO) that corrections to this approximation, named hereafter as "full recoil," are numerically irrelevant in spectral calculations (not shown).

We also consider a less accurate approximation, dubbed as "midrecoil," whereby the midpoint of the interval in Eq. (10) is taken as a proxy for E_e [84],

$$E_e \simeq E_e^{\text{mid}} = (E_1 + E_2)/2, \tag{12}$$

and the Jacobian,

$$J(E) = (dE_e^{\text{mid}}/dE)^{-1}, \tag{13}$$

is included, when passing from neutrino to positron energy spectra, to ensure event number conservation. A useful approximation for E_e^{mid} (and thus for J) is given in [84] as

$$E_e^{\text{mid}}(E) \simeq \frac{E - \Delta_E}{1 + \frac{E}{m_p}}, \tag{14}$$

$$J(E) \simeq \frac{(1+\frac{E}{m_p})^2}{1+\frac{\Delta_E}{m_p}}, \tag{15}$$

where $\Delta_E = m_e + 0.783$ MeV. This midrecoil recipe captures well the average recoil shift but ignores its energy spread, which is definitely non-negligible in TAO as shown below.

C. Resolution and recoil effects: Comparison and combination

If both resolution and recoil effects were neglected, then Eqs. (6) and (9) would lead to the often-quoted approximation $E_{\rm vis} = E - 0.783$ MeV. Figure 1 (left panel) shows the recoil corrections to such relation as a function of neutrino energy E, in terms of deviations from unity [dashed line at $1 \equiv E_{\rm vis}/(E - 0.783\ {\rm MeV})$]. The gray area corresponds to the one-sided energy deficit due to full recoil effects [Eq. (10)], while the solid line marks the midrecoil approximation [Eq. (12)]. Notice that, at high reactor neutrino energies, the visible event energy is both shifted and smeared out at the percent level. In Fig. 1 (right panel), we show the fractional energy spread $\Delta E_{\rm vis}/E_{\rm vis}$ due to recoil and resolution, separately. In particular, $\Delta E_{\rm vis}$ is shown as $\pm(E_2 - E_1)/2$ for recoil (dark gray), as $\pm\sigma_T$ for TAO (gray band) and as $\pm\sigma_J$ for JUNO (light gray). Recoil and resolution effects in TAO appear to be of comparable size, and none of them can be neglected in accurate spectral analyses, especially in view of their impact on the observability of substructures.

As shown in [77], the combination of the resolution and recoil effects is fully encoded in an energy resolution function R_X that connects the relevant energies $E_{\rm vis}$ and E, as obtained by convolving the Gaussian distribution r_X in Eq. (7) with the top-hat distribution t in Eq. (11),

$$\begin{aligned} R_X(E_{\rm vis}, E|\sigma_X^2) &= r_X * t \\ &= \frac{1}{2(E_2 - E_1)}\left[{\rm erf}\left(\frac{E_{\rm vis} - (E_1 + m_e)}{\sqrt{2\sigma_X^2}}\right)\right. \\ &\quad \left. - {\rm erf}\left(\frac{E_{\rm vis} - (E_2 + m_e)}{\sqrt{2\sigma_X^2}}\right)\right], \end{aligned} \tag{16}$$

where $\sigma_X = \sigma_X(E_{\rm vis})$, while the dependence on E comes from $E_{1,2} = E_{1,2}(E)$ that we take from the full calculation in [83]; see [77] for further details, including the adopted convention for the error function (erf).

The observable energy spectra S_X of IBD events in TAO and JUNO (in the absence of oscillations) can then be computed by convolving the neutrino spectrum S_ν in Eq. (3) with the above resolution function,

$$\begin{aligned} S_X(E_{\rm vis}) &= \mathcal{N}_X S_\nu * R_X \\ &= \mathcal{N}_X \int_{E_T}^{\infty} dE\, S_\nu(E)\, R_X\,(E_{\rm vis}, E|\sigma_X^2),\ X = T, J, \end{aligned} \tag{17}$$

where $E_T = 1.806$ MeV is the IBD ν energy threshold and $\mathcal{N}_X$ is a normalization factor.

Figure 2 shows in the left panel the neutrino energy spectrum S_ν, as obtained with default nuclear input parameters for the ν flux Φ from the Oklo toolkit [79], times the cross section from [83]. The TAO visible energy spectrum S_T is shown in the right panel, including recoil and energy resolution effects. Spectra are normalized to the same area (in arbitrary units) to facilitate comparison in shape. It can be seen that spectral substructures in S_ν (sawtooth and step-like features) are smeared out in S_T, but still partly visible. Such substructures would no longer be visible in JUNO (not shown).

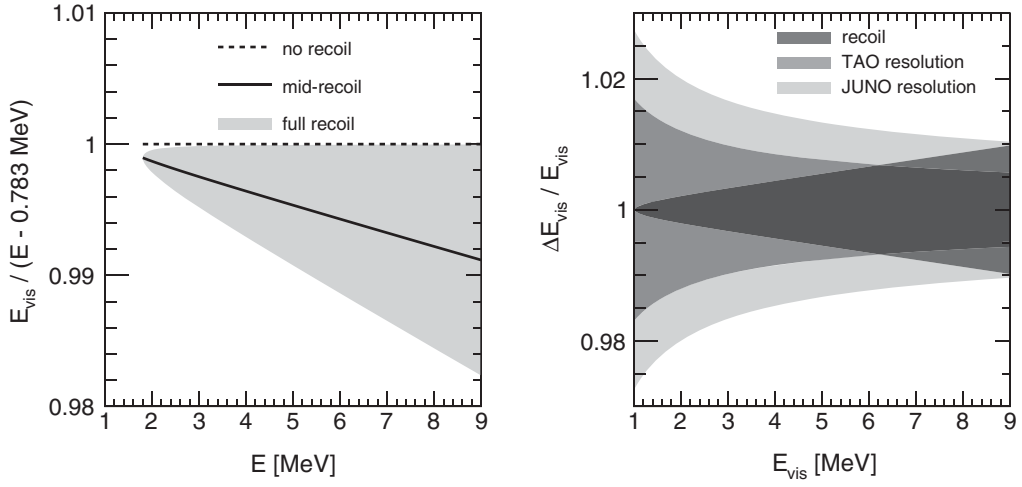

FIG. 1. Left panel: fractional recoil effects in terms of neutrino energy. Right panel: energy spread due to recoil, compared with 1σ resolution widths in TAO and JUNO. In both panels, the recoil band is bounded by kinematical limits. See the text for details.

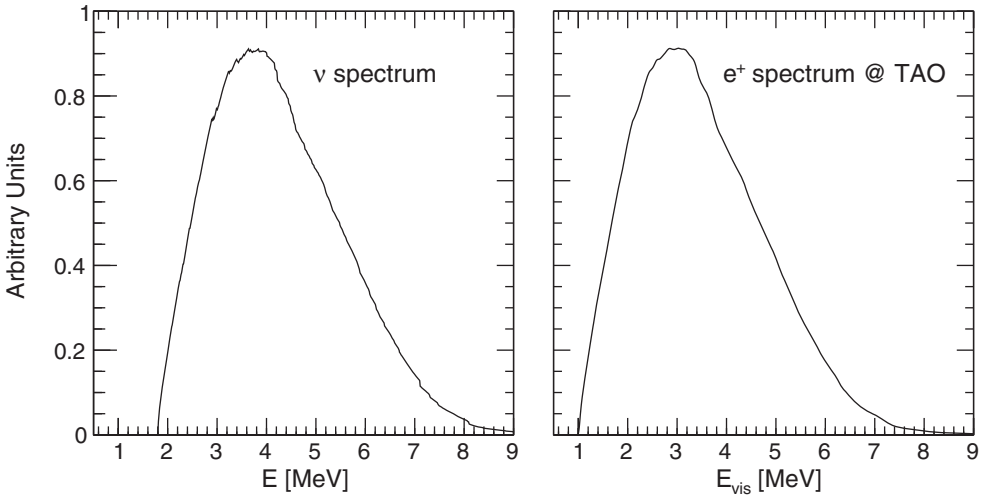

FIG. 2. Reference neutrino spectrum as obtained from the Oklo toolkit [79] (left panel) and corresponding visible energy spectrum at TAO, including recoil and resolution effects (right panel). For graphical comparison, the two spectra are normalized to the same area, in arbitrary units.

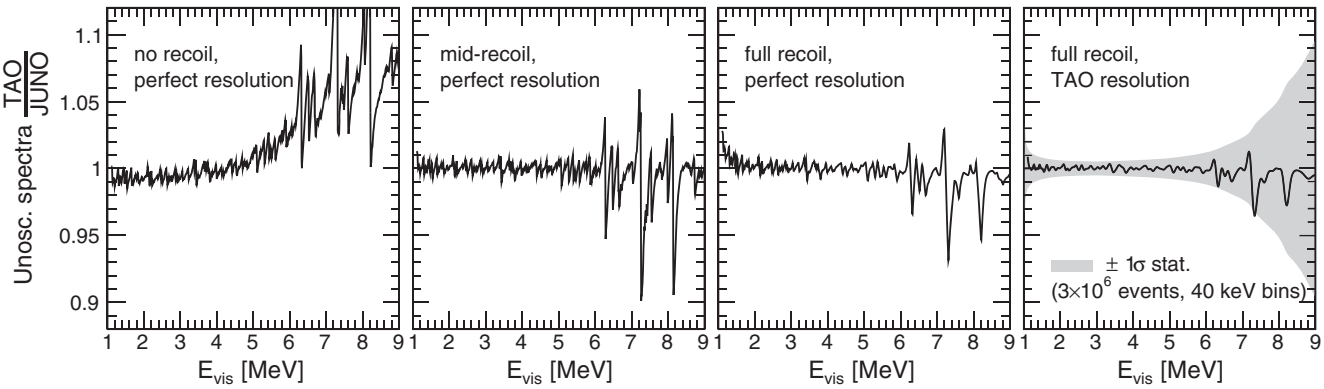

FIG. 3. Ratio S_T/S_J of visible energy spectra in TAO and JUNO (unoscillated), normalized to the same area for comparison. The denominator S_J always include full recoil and resolution effects. The numerator S_T includes recoil and resolution effects in progression from left to right. In the rightmost plot, the spectral ratio substructures are compared with the ± 1 statistical error band in TAO, assuming 3×10^6 events and 40 keV bin width.

Figure 3 shows the ratio S_T/S_J of the unoscillated energy spectra in TAO and JUNO (arbitrarily normalized to the same area). From left to right, the numerator S_T is calculated with progressive inclusion of recoil and resolution effects, while the denominator S_J always includes all such effects. In particular, the first three panels assume perfect energy resolution in TAO ($\sigma_T = 0$), with increasingly accurate treatments for nucleon recoil. In the first plot (no recoil), the spectral ratio shows evident substructures and a high-energy excess (spectral tilt), due to neglected energy recoil losses that also bias the substructure peak positions by up to 1% (not visible by eye). In the second plot (midrecoil approximation including the Jacobian), the average energy losses are accounted for, the shift disappears, and the substructures are correctly aligned in energy. In the third plot (full recoil treatment), the inclusion of the recoil energy spread suppresses the finest spectral structures and, at high energy, reduces their amplitudes by a factor of ∼2. Finally, further suppression of fine structure features (and another amplitude reduction by a factor of ∼2 or more) is due to the inclusion of the finite TAO resolution width σ_T from Eq. (8) in the rightmost panel. In this panel, we also show the $\pm 1\sigma$ error band in TAO assuming 3×10^6 events, i.e., ∼30 times the statistics expected in JUNO [67] in the presence of oscillations for about 5 years (that amounts to ∼100, 000 events [77]). The statistical band depends on the bin width, here taken as 40 keV (25 bins per MeV interval) in order to cover the most prominent substructures within a few bins at least. It can be seen that a handful of fine-structure features reach the $\sim 1\sigma$ level in amplitude, allowing TAO to probe spectral models with different predicted substructures (see also [67]). We shall discuss some statistical issues concerning the model selectivity of TAO in Sec. V.

Summarizing, resolution and recoil effects in the TAO energy spectrum are of comparable size and should be carefully implemented, in order to avoid energy biases and unrealistic amplitudes for fine-structure spectral features. Resolution effects produce a Gaussian smearing (whose width decreases with increasing energy), while recoil effects produce an energy shift plus a top-hat smearing (whose width increases with increasing energy). Their combination (convolution) leads to an analytical expression for the energy resolution function [77] as in Eq. (16), that can be usefully applied to the calculation of both TAO and JUNO spectra.

Finally, we mention that, in principle, the impact of recoil effects may be reduced by directional information in the final state of IBD events; see [85] for a recent proposal in the context of TAO. We do not explore this option hereafter, but surmise that constraining recoil effects amounts to replace the function t in Eq. (11) with another one (t') having smaller variance, possibly leading to an analytical result as in Eq. (16) if the parametrization of t' is simple.

D. Mapping the spectrum from near to far

The resolution function R_J in Eq. (16) for JUNO is obtained by convolving a Gaussian r_J having a variance σ_J^2 with a top-hat function t. In turn, r_J can be thought as the convolution of two Gaussians r_T and r_D with variances given, respectively, by σ_T^2 (as in TAO) and by

$$\sigma_D^2(E_{\rm vis}) = \sigma_J^2(E_{\rm vis}) - \sigma_T^2(E_{\rm vis}) > 0, \tag{18}$$

that is, the difference between the energy resolution variances in JUNO and TAO.

Then, through convolutions, one gets an exact mapping from TAO to JUNO (unoscillated) spectra as follows:

$$\begin{aligned} S_J(E_{\rm vis}) &= S_\nu * R_J \\ &= S_\nu * r_J * t \\ &= S_\nu * r_D * r_T * t \\ &= S_J * r_D \\ &= \int_0^\infty dE'_{\rm vis} S_J(E'_{\rm vis}) r_D(E_{\rm vis}, E'_{\rm vis}|\sigma_D^2), \end{aligned} \tag{19}$$

where normalization factors $\mathcal{N}_X$ have been dropped for simplicity, and r has the same functional form as in Eq. (7), with $E_e + m_e$ replaced by $E'_{\rm vis}$.

This analytical result has a simple physical interpretation: the JUNO unoscillated spectrum in visible energy (S_J) can be obtained from the TAO spectrum (S_T) by applying an extra Gaussian smearing with variance σ_D^2, equal to the difference of variances in JUNO (σ_J^2) and TAO (σ_T^2). In doing so, recoil effects remain correctly implemented in both TAO and JUNO.

Note that Eq. (19) directly relates the observable event spectra S_T and S_J, without using the unobservable neutrino spectrum S_ν. This represents an advantage in terms of nuclear physics modeling: Constructing a model for S_T (compatible with future TAO data) will generally be less demanding than building a complete model for S_ν, since the former will exhibit only a few surviving substructures to be properly described via summation.

A final comment is in order. As stated in Sec. I, we are assuming the TAO and JUNO spectra are generated by the same underlying ν spectrum S_ν. However, JUNO will collect a neutrino flux also from reactor cores different from the one monitored by TAO, leading to fuel-component differences in the reference S_ν and to corrections to the ideal case in Eq. (19). Fuel evolution issues and related spectral effects in TAO versus JUNO are beyond the scope of this investigation and will be treated in a future work; see [67,72,81] for useful considerations in this context.

III. MAPPING THE SPECTRUM FROM TAO TO JUNO WITH OSCILLATIONS

In this section, we generalize the TAO → JUNO mapping of Eq. (19) in the presence of oscillations, characterized by a $\bar{\nu}_e$ survival probability $P_{ee}(E)$. An obstacle to this goal is that the integrand $S_\nu(E)$ gets replaced by the product $S_\nu \cdot P_{ee}$ in JUNO, and that the convolution of a product is not the product of convolutions, as also noted in [81].

However, after reviewing the functional form of P_{ee}, we propose an ansatz that, to a very good approximation, overcomes this problem. We shall generalize Eq. (19) by including an effective probability $P_{ee}^{\rm eff}$, expressed in terms of observable spectra S_X and visible energy $E_{\rm vis}$, that bypasses any prior knowledge of the (unobservable) neutrino energy spectrum $S_\nu(E)$. We shall then discuss the validity of this ansatz and use it in an updated analysis of the JUNO sensitivity to the neutrino mass ordering and to precision oscillometry.

A. Oscillation probability in terms of neutrino energy

In this subsection, we describe the survival probability $P_{ee}(E)$, largely following [77] to which we refer the reader for details and references. In general, $P_{ee}(E)$ in JUNO depends on several parameters,

$$P_{ee}(E) = P_{ee}(E|\delta m^2, \Delta m^2, \alpha, \theta_{12}, \theta_{13}, N_e, \{w_n, L_n\}), \tag{20}$$

where $\delta m^2 = m_2^2 - m_1^2$ and $\Delta m^2 = |m_3^2 - (m_1^2 + m_2^2)/2| > 0$ are the squared mass splitting parameters, $\alpha = \pm 1$ distinguishes the mass ordering (normal or inverted), θ_{12} and θ_{13} are the mixing angles, N_e is the electron density in matter, and $\{w_n, L_n\}$ characterizes the set of reactors, each contributing to the total flux with fractional weight w_n

($\sum_n w_n = 1$) at distance L_n, under the assumption of identical fuel components.

Useful derived parameters are

$$\Delta m^2_{ee} = \Delta m^2 + \frac{\alpha}{2}(c^2_{12} - s^2_{12})\delta m^2, \tag{21}$$

where $c_{12} = \cos\theta_{12}$ and $s_{12} = \sin\theta_{12}$, and

$$\delta = \frac{\delta m^2 L}{4E}, \qquad \Delta_{ee} = \frac{\Delta m^2_{ee} L}{4E}, \tag{22}$$

where $L = \sum_n w_n L_n$ is the average baseline. Matter effects in JUNO depend on the ratio $\mu = (2\sqrt{2}G_F N_e E)/\delta m^2$ and lead to an effective mass-mixing pair $(\tilde{\delta}, \tilde{\theta}_{12})$ given by $\tilde{\delta} \simeq \delta(1 + \mu\cos 2\theta_{12})$ and $\sin 2\tilde{\theta}_{12} \simeq \sin 2\theta_{12}(1 - \mu\cos 2\theta_{12})$ at first order in the small parameter μ [77] (see also [86,87]). The dependence of P_{ee} on its parameters can then be simply expressed as

$$P_{ee}(E) = c^4_{13}\tilde{P} + s^4_{13} + 2s^2_{13}c^2_{13}\sqrt{\tilde{P}}w\cos(2\Delta_{ee} + \alpha\varphi), \tag{23}$$

where

$$\tilde{P} = 1 - 4\tilde{s}^2_{12}\tilde{c}^2_{12}\sin^2\tilde{\delta} \tag{24}$$

encodes $(\tilde{\delta}, \tilde{\theta}_{12})$ matter effects, while $w \simeq 1\text{–}2\Delta^2_{ee}\sum_n w_n (1 - L_n/L)^2$ is a damping factor due to the spread of baselines L_n, and φ is the interference phase directly related to mass ordering [88]. An accurate empirical parametrization for φ is given by [77][2]

$$\varphi \simeq 2s^2_{12}\delta\left(1 - \frac{\sin 2\delta}{2\delta\sqrt{P}}\right), \tag{25}$$

where P reads as in Eq. (24) but with vacuum mass-mixing values (δ, θ_{12}).[3]

For the oscillation parameters in P_{ee} [Eq. (23)], we assume the following priors (central values and $\pm 1\sigma$, after symmetrizing errors and averaging NO-IO differences) from the global analysis in [89]

$$s^2_{12} = (3.04 \pm 0.13) \times 10^{-1}, \tag{26}$$

$$\delta m^2 = (7.34 \pm 0.16) \times 10^{-5}\ \text{eV}^2, \tag{27}$$

$$s^2_{13} = (2.16 \pm 0.08) \times 10^{-2}, \tag{28}$$

$$\Delta m^2_{ee} = (2.448 \pm 0.034) \times 10^{-3}\ \text{eV}^2. \tag{29}$$

[2]Here we report a typo in Eq. (45) of [77], where $\sin\delta$ should be replaced by $\sin 2\delta$. We thank A. Formozov for detecting the misprint.

[3]Replacing (δ, P) with $(\tilde{\delta}, \tilde{P})$ in φ leads to insignificant corrections to P_{ee} [77].

Determining the mass ordering in JUNO amounts to prove that in P_{ee}, besides the oscillation phase $2\Delta_{ee}$, there is an extra interference phase φ endowed with a definite sign ($\alpha = \pm 1$) and not scaling as $1/E$; otherwise, it would be absorbed into a shift of Δm^2_{ee} [90]; equivalently, one should find evidence for a nonconstant ratio $\varphi/2\Delta_{ee}$. It has been pointed out [91] that energy calibration errors at (sub)percent level may (partly) mimic $\varphi/2\Delta_{ee} \neq$ const [15,77,78]; in this context, future evidence for some substructures emerging in TAO spectrum, located at the energies predicted by nuclear summation models, may help the overall calibration of the reference spectrum to be projected from TAO to JUNO (provided that JUNO is also accurately calibrated in energy).[4] Correct implementation of recoil effects, in both TAO and JUNO, remains mandatory to avoid energy biases at comparable (sub)percent levels.

Figure 4 shows the function P_{ee} (left panel) and the ratio $\varphi/2\Delta_{ee}$ (right panel) as a function of energy. The solid curves and gray bands correspond, respectively, to the central values and to the envelopes of $\leq 1\sigma$ variations for the oscillation parameters. Normal ordering is assumed. The smallness of $\varphi/2\Delta_{ee}$, and the fact that its variations are limited to a relatively small energy range between about 2 and 4 MeV, illustrates the challenges of mass ordering determination at MBL reactors. Note the relatively high values of $\varphi/2\Delta_{ee}$ for $E \sim 3$ MeV may fractionally change by up to $\pm 8\%$ within the gray band, and that for similar energies P_{ee} (and thus the IBD event rate) may also change by up to $\pm 12\%$. Therefore, variations of the oscillation parameters within their current global-fit errors can appreciably affect the prospective mass ordering sensitivity in JUNO, as discussed later.

B. Ansatz: Effective probability in terms of visible energy

Given the probability $P_{ee}(E)$, the oscillated spectrum at JUNO (including resolution and recoil effects, and up to a normalization factor) is

$$S_J(E_{\text{vis}}) = \int_{E_T}^{\infty} dE\, S_\nu(E)\, P_{ee}(E)\, R_J(E_{\text{vis}}, E|\sigma^2_J). \tag{30}$$

Our goal is to obtain such S_J by mapping the TAO spectrum S_T, in a form analogous to Eq. (19),

$$S_J(E_{\text{vis}}) = \int_0^{\infty} dE'_{\text{vis}}\, S_T(E'_{\text{vis}})\, P^{\text{eff}}_{ee}(E'_{\text{vis}})\, r_D(E_{\text{vis}}, E'_{\text{vis}}|\sigma^2_D), \tag{31}$$

[4]It should be noted that the uncertainties on Δm^2_{ee} and on energy scale assumed in this work are definitely smaller (by a factor of a few) than those adopted in [91] to suppress or swap hierarchy effects.

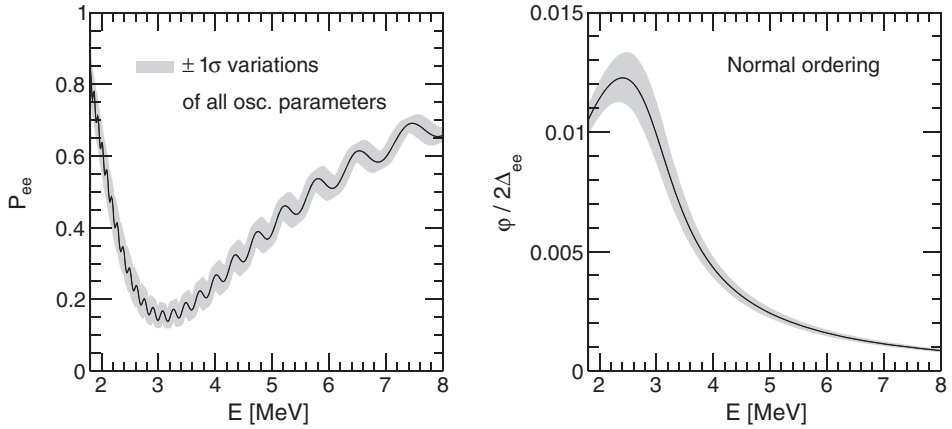

FIG. 4. Survival probability P_{ee} (left panel) and oscillation phase ratio $\varphi/2\Delta_{ee}$ (right panel) for electron antineutrinos with energy E in JUNO. Solid lines are computed for central values of the oscillation parameters, while the gray bands correspond to the envelope of $\leq 1\sigma$ variations in the prior ranges (see the text). Normal ordering is assumed. For inverted ordering, P_{ee} would be similar while $\varphi/2\Delta_{ee}$ would reverse its sign (not shown).

where $P_{ee}^{\rm eff}$ should act as an effective oscillation probability, expressed in terms of the measured visible energy rather than the unobservable neutrino energy. This problem is *exactly* solved by imposing, in the kernel of Eq. (31), that

$$S_T(E'_{\rm vis})\, P_{ee}^{\rm eff}(E'_{\rm vis}) = \int_{E_T}^{\infty} dE\, S_\nu(E)\, P_{ee}(E)\, R_T(E'_{\rm vis}, E|\sigma_T^2), \tag{32}$$

namely, by defining $P_{ee}^{\rm eff}$ as follows (with a change $E'_{\rm vis} \to E_{\rm vis}$ in the dummy variable):

$$P_{ee}^{\rm eff}(E_{\rm vis}) = \frac{\int_{E_T}^{\infty} dE\, S_\nu(E)\, P_{ee}(E)\, R_T(E_{\rm vis}, E|\sigma_T^2)}{\int_{E_T}^{\infty} dE\, S_\nu(E)\, R_T(E_{\rm vis}, E|\sigma_T^2)}, \tag{33}$$

which represents the weighted average of P_{ee} over the neutrino spectrum (S_ν) times the TAO energy resolution function (R_T). In a sense, $P_{ee}^{\rm eff}$ is a smeared version of P_{ee}, averaged over S_ν variations on an energy scale set by σ_T.

However, this formally exact solution is not satisfactory, as it requires the knowledge of the unobservable neutrino spectrum S_ν. We make then the following ansatz, that replaces the unobservable S_ν with its closest observable proxy, namely, S_T: within the integral kernels of Eq. (33), the function $S\nu(E)$ is substituted by the TAO spectral function $S_T(E_{\rm vis})$, and in turn $E_{\rm vis}$ is identified with its closest proxy $E_{\rm vis}(E) = E_e^{\rm mid}(E) + m_e$. Conservation of number of events is ensured by imposing $S_\nu(E)dE = S_T(E_e^{\rm mid} + m_e)dE_e^{\rm mid}$, so that the complete replacement involves $J^{-1}(E) = dE_e^{\rm mid}/dE$,

$$S_\nu(E) \to S_T(E_e^{\rm mid}(E) + m_e))J^{-1}(E). \tag{34}$$

The effect of the Jacobian in the above formula is rather small numerically, since $J(E)$ changes slowly with E (if it were constant, it would be canceled in the ratio); we keep it for the sake of completeness.

Summarizing, our ansatz for the mapping $S_T \to S_J$ (including oscillations) consists of calculating an effective JUNO spectrum $S_J^{\rm eff}(E_{\rm vis})$ from the observable TAO spectrum $S_T(E_{\rm vis})$ as

$$S_J^{\rm eff}(E_{\rm vis}) = \int_0^{\infty} dE'_{\rm vis}\, S_T(E'_{\rm vis})\, P_{ee}^{\rm eff}(E'_{\rm vis})\, r_D(E_{\rm vis}, E'_{\rm vis}|\sigma_D^2), \tag{35}$$

via the effective probability

$$P_{ee}^{\rm eff}(E_{\rm vis}) \simeq \frac{\int_{E_T}^{\infty} dE\, S_T(E_e^{\rm mid} + m_e)\, J^{-1}(E)\, P_{ee}(E) R_T(E_{\rm vis}, E|\sigma_T^2)}{\int_{E_T}^{\infty} dE\, S_T(E_e^{\rm mid} + m_e)\, J^{-1}(E)\, R_T(E_{\rm vis}, E|\sigma_T^2)}. \tag{36}$$

In the limit of no oscillations ($P_{ee} = 1 = P_{ee}^{\rm eff}$), Eq. (35) reproduces the exact result in Eq. (30). We surmise that this recipe can approximately capture the local smearing of P_{ee} implicit in Eq. (33) without introducing energy biases, as the average recoil effects are accounted for by the midrecoil approximation. Of course, the replacement of $S_\nu(E)$ with the proxy $S_T(E_e^{\rm mid}(E) + m_e)$ introduces an extra smearing associated to the latter spectrum, which is absent in the former. This artifact may be expected to have marginal effects in the final S_J, since the smearing in JUNO acts on an energy scale $\sigma_J > \sigma_T$. Ultimately, the validity of our ansatz relies on numerical tests.

Figure 5 shows the ratio of the JUNO spectra calculated with the ansatz [$S_J^{\rm eff}$ from Eqs. (35) and (36)] and without the ansatz [S_J from Eq. (30)]. The underlying neutrino spectrum S_ν is taken as the reference Oklo spectrum in

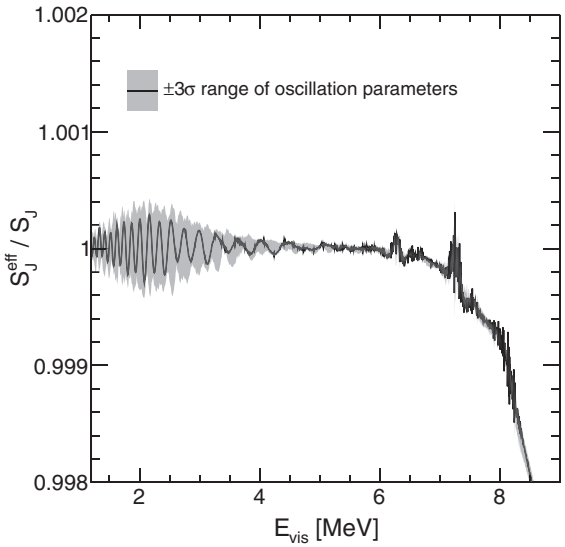

FIG. 5. Accuracy of the mapping $S_T \to S_J$ in the presence of oscillations: Ratio of JUNO energy spectra calculated with the ansatz $(S_J^{\rm eff})$ and without it (S_J). The solid line is computed for central values of the oscillation parameters, while the gray band corresponds to the envelope of $\leq 3\sigma$ variations in the prior ranges. Normal ordering is assumed. See the text for details.

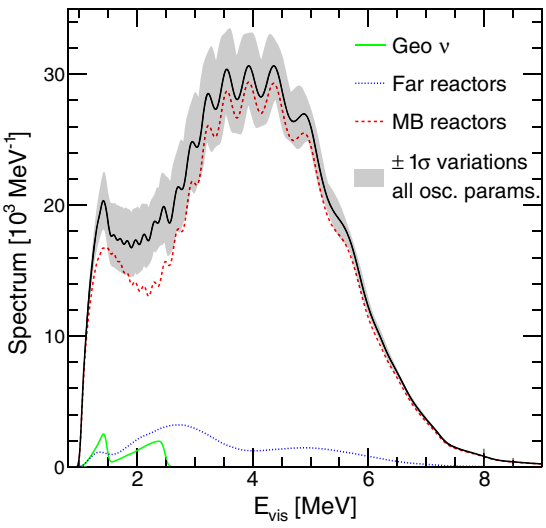

FIG. 6. Absolute energy spectrum of IBD events expected after 5 years in JUNO, for oscillation parameters taken at their central value (black solid line) or left free within $\leq 1\sigma$ (gray envelope). Normal ordering is assumed. The breakdown of the total spectrum in its three components (MBL reactors, far reactors, and geoneutrinos) is also shown. The red dashed line corresponds to the spectrum S_J discussed in the text.

Fig. 1 (left panel). The solid line and gray band refer, respectively, to central values of the oscillation parameters and to their $\pm 3\sigma$ variations (applied to both $S_J^{\rm eff}$ and S_J at the same time). The ansatz provides numerically accurate results at the level of few $\times 10^{-4}$, except in the high-energy tail where it reaches a permill level, that is anyway insignificant as compared with other sources of uncertainties (both statistical and systematic) in JUNO, as also discussed below. Finally, we have tested that the same excellent accuracy in Fig. 5 is reached by replacing the reference spectrum with variant spectra, as obtained from the Oklo toolkit by changing the nuclear inputs within their uncertainties (not shown).

IV. NEUTRINO OSCILLOMETRY IN JUNO: SINGLE SPECTRUM

We present and discuss a prospective analysis of JUNO in terms of sensitivity to mass ordering and of precision determination of oscillation parameters, building upon our previous work [78]. Here we use a single input spectrum, namely, the reference Oklo one as shown in the previous sections. Bundles of variant spectra and their effects will be considered in the next section. The main purpose of this updated analysis is to further test the previous ansatz and to discuss the impact of changes in the reference oscillation parameters and other systematics. TAO does not play a specific role herein, except for providing a reference spectrum S_T for the $S_T \to S_J$ mapping, when the ansatz is used.

A. Ingredients of the analysis

Figure 6 shows the observable JUNO spectrum S_J expected in the presence of oscillations from the Taishan and Yangjiang reactor sources (dashed red line) plus the background components expected from farther reactors (blue dotted line) and U + Th geoneutrinos (green solid line).[5] The total spectrum (black solid line) is endowed with a gray band, representing the envelope of variations of the oscillation parameters within their prior 1σ ranges. All curves refer to 5 years of data taking ($\sim 10^5$ JUNO events), assuming the same normalization factors for the various components as discussed in [78], to which we refer the reader for details not repeated herein.

We focus here on the inputs that differ from [78]. The central values (and to some extent the errors) of the oscillation parameters in Eqs. (26)–(29) have changed, in particular for the mass splittings (about $+1\sigma$ for Δm^2_{ee} and -1σ for δm^2_{ee}). Concerning Φ, we use the reference neutrino flux from the Oklo toolkit, corresponding to the neutrino spectrum $S_\nu = \Phi\sigma_\nu$ in Fig. 1 (left panel). Note that, in this section, we do not attach uncertainties to the fine structures of Φ, that will be separately addressed in Sec. V. However, we do include large-scale (smooth) uncertainties of the flux shape in the form of polynomial deviations Φ'/Φ, as well as energy-scale systematics in the

[5]The double-peaked (U + Th) structure of the geo-ν spectrum is a peculiar realization of sawtooth substructures in summation spectra.

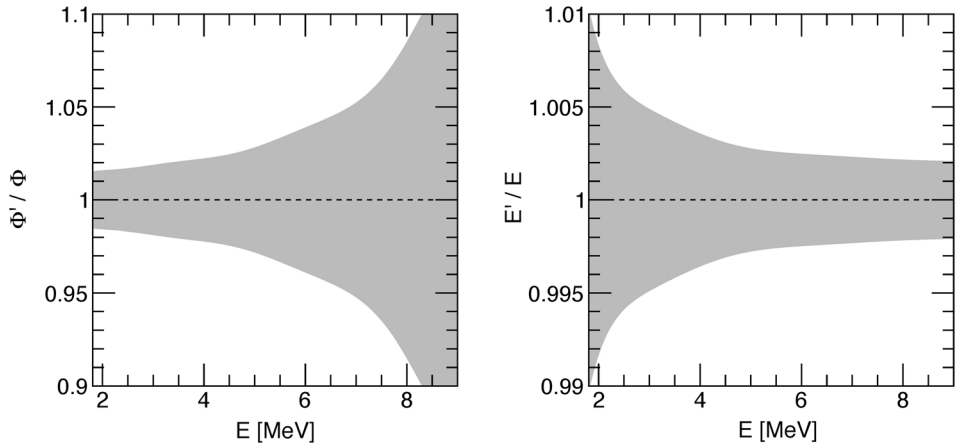

FIG. 7. Error bands ($\pm 1\sigma$) assumed for flux-shape variations Φ'/Φ (left panel) and energy-scale variations E'/E in JUNO.

form of polynomial deviations E'/E, adopting the same methodology as in [78] but with narrower error bands.

Figure 7 shows our default $\pm 1\sigma$ error bands for Φ'/Φ and E'/E variations (left and right panels, respectively). Here we reduce the width of the Φ'/Φ band to 2/3 of the previously adopted one in [78], because (1) at low energy, the normalization error (that sets the lower limit to the width) has been reduced from ~2.3% [78] to ~1.5% [28]; at high energies, prospective analyses of the flux-shape reconstruction in TAO [67] give reasons for moderate optimism. The E'/E error band is taken from [92] (see Fig. 18 therein), with an appreciable reduction (roughly by a factor 1/2) with respect to [78].

B. Sensitivity to mass ordering

Following [78], we perform a least-squares analysis of the JUNO sensitivity to mass ordering, up to 10 years of data taking. We remind that our complete χ^2 function for JUNO is defined as

$$\chi^2_{\rm JUNO} = \chi^2_{\rm stat} + \chi^2_{\rm par} + \chi^2_{\rm sys}, \tag{37}$$

where the first term includes statistical errors only; the second term includes penalties for variations of the oscillation parameters, governed by the priors in Eqs. (26)–(29); the third term contains normalization errors for the geo-ν Th and U fluxes, normalization and (polynomial) shape systematics for the reactor fluxes, and (polynomial) energy-scale systematics. The second and third terms contain up to $N_{\rm sys} = 18$ systematics, treated as nuisance parameters that are marginalized away in the χ^2_J minimization [78]. The analysis is performed by progressively including such nuisance parameters: (1) oscillation parameters and normalizations (osc. + norm.), $N_{\rm sys} = 7$; (2) plus energy-scale variations, $N_{\rm sys} = 13$; (3) plus flux-shape variations, $N_{\rm sys} = 18$. Normal (inverted) ordering is assumed as true (test) hypothesis.

Figure 8 shows the results of the JUNO analysis in terms of standard deviations [$N_\sigma = \sqrt{\Delta\chi^2(\mathrm{IO} - \mathrm{NO})}$] as a function of the detector live time T, with tic marks scaling as $\sqrt{T}$. Solid lines refers to the standard calculation of S_J from S_ν, while dashed lines to the approximate $S_T \to S_J$ mapping; the excellent agreement corroborates the validity of our ansatz. The statistical rejection of the wrong IO reaches $2-3\sigma$ in 5–10 years, depending on systematic errors. Note that systematics do not seem to saturate the sensitivity to mass ordering even with the 10-year data. Also, note that this sensitivity is reduced more by energy-scale uncertainties than by flux-shape ones. Therefore,

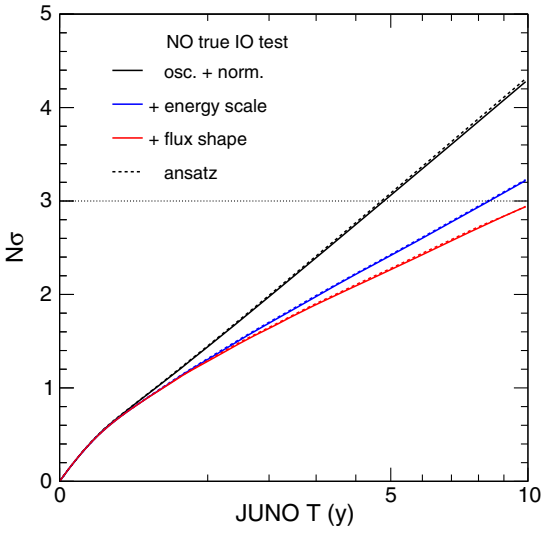

FIG. 8. JUNO analysis: statistical significance of the rejection of inverted ordering (IO, test hypothesis) with respect to normal ordering (NO, true hypothesis), as a function of the live time T, including different sets of systematics: oscillation and normalization uncertainties (black), plus energy-scale uncertainties (blue) plus flux-shape uncertainties (red). Dashed lines refer to the calculation of the JUNO spectrum by mapping the TAO spectrum (ansatz discussed in the text).

it will be important to ensure that the energy calibration in JUNO can achieve the same (or better) level of accuracy reached in [28].

It is useful to compare Fig. 8 with the analogous Fig. 7 in [78]. It turns out that the curve $N_\sigma(T)$ including the full set of systematics (red curve) is almost unaltered, despite the previously discussed reduction in energy-scale and flux-shape systematics. The (surprising to us) explanation is that the benefits of this error reduction happen to be accidentally compensated by "unlucky" changes in the central values of the oscillation parameters. Further understanding can be gained by focusing on the case with "osc. + norm." errors only (black curve in Fig. 8) for a fixed live time $T = 5$ years.

Figure 9 shows how the $\Delta\chi^2(\mathrm{IO}-\mathrm{NO})$ changes by varying the central values of the oscillation parameters, with respect to those reported in Eqs. (26)–(29) and marked by a star. The left panel shows $\Delta\chi^2$ variations (isolines) in the plane $(\delta m^2, \sin^2\theta_{12})$ for fixed $(\Delta m^2_{ee}, \sin^2\theta_{13})$ and vice versa in the right panel. The coordinates span the $\pm 2\sigma$ ranges for the mass splitting and $\pm 1\sigma$ ranges for the mixing angles in the units of Eqs. (26)–(29). The $\Delta\chi^2$ value increases noticeably by increasing δm^2 or by decreasing Δm^2; in other words, the mass ordering test in JUNO improves when the ratio $\rho = \delta m^2/\Delta m^2_{ee}$ increases, even if by small amounts (conversely, the mass ordering would become eventually untestable for vanishing ρ). Note that an (more modest) increase of $\Delta\chi^2$ is also obtained by increasing either $\sin^2\theta_{12}$ or $\sin^2\theta_{13}$ and thus the oscillation amplitude(s), as it can be generally expected in oscillation searches.

It turns out that, with respect to [78], the central values of all four oscillation parameters in Eqs. (26)–(29) have accidentally changed in unlucky directions, lowering $\Delta\chi^2$ by about 3.5 units for the case of osc. + norm. uncertainties. As anticipated, for the analysis including all the uncertainties, this drop is almost exactly compensated (once more, accidentally) by the reduction of energy-scale and flux-shape systematics. Similar results have been obtained in the case where the true ordering is inverted and NO is tested (not shown). In conclusion, the JUNO rejection of the wrong mass ordering depends, in a non-negligible way, on the central values of the oscillation parameters.

C. Accuracy of oscillation parameters

Eventually, at least three oscillation parameters (δm^2, $\Delta m^2_{ee}, \theta_{12}$) will be very precisely measured by JUNO itself. Figure 10 shows the time evolution (in JUNO) of the fractional accuracy σ_p/p for each of six parameters p, namely, from top to bottom: the two mass splittings, the two mixing angles, and the U and Th geoneutrino flux normalizations (f_{U} and f_{Th}). For each parameter, it is understood that the others are marginalized away in the analysis. At $T = 0$, the oscillation parameter errors are set by Eqs. (26)–(29), while for the geo-ν fluxes we assume the priors in [78], $f_{\mathrm{U}} = 1 \pm 0.20$ and $f_{\mathrm{Th}} = 1 \pm 0.27$. The color sequence for the curves (red, blue, and black for growing sets of systematics) is the same as in Fig. 8. After a live time of 5 years, the accuracy of $(\delta m^2, \Delta m^2_{ee}, \theta_{12})$ will improve by factors of about (6,6,4), respectively—or better, if some systematics can be further reduced. For the pair $(\delta m^2, \Delta m^2_{ee})$, that governs the "slow" oscillations in the JUNO spectrum, flux-shape uncertainties are more important than energy-scale ones, and vice versa for Δm^2_{ee} that governs the "fast" oscillations. A moderate reduction of the prior errors will be obtained for geoneutrino fluxes, with little dependence on systematics. Concerning θ_{13}, the current experimental error will only be marginally

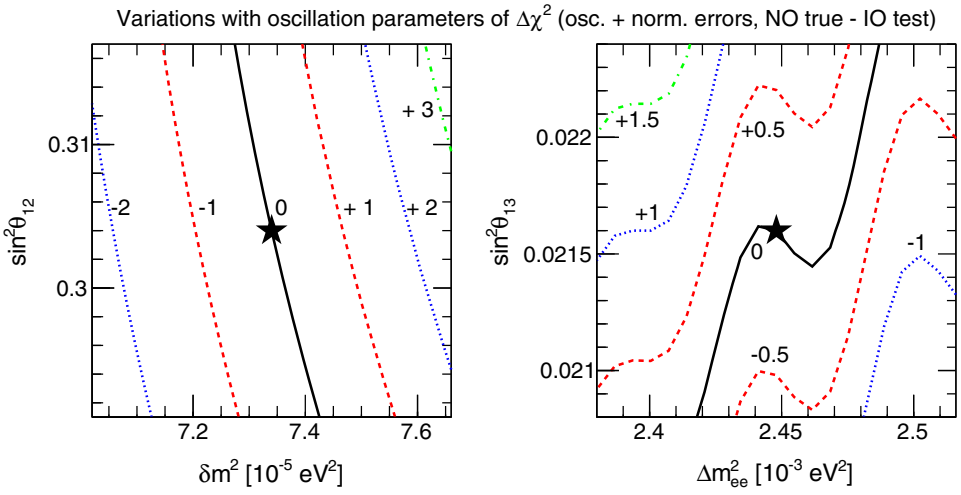

FIG. 9. JUNO analysis: isolines of $\Delta\chi^2$ variations for the test of IO (assuming true NO), including only oscillation and normalization errors. The left and right planes are charted by $(\delta m^2, \sin^2\theta_{12})$ and $(\Delta m^2_{ee}, \sin^2\theta_{13})$, respectively. The central values of the oscillation parameters are marked by a star. Results refer to $T = 5$ years.

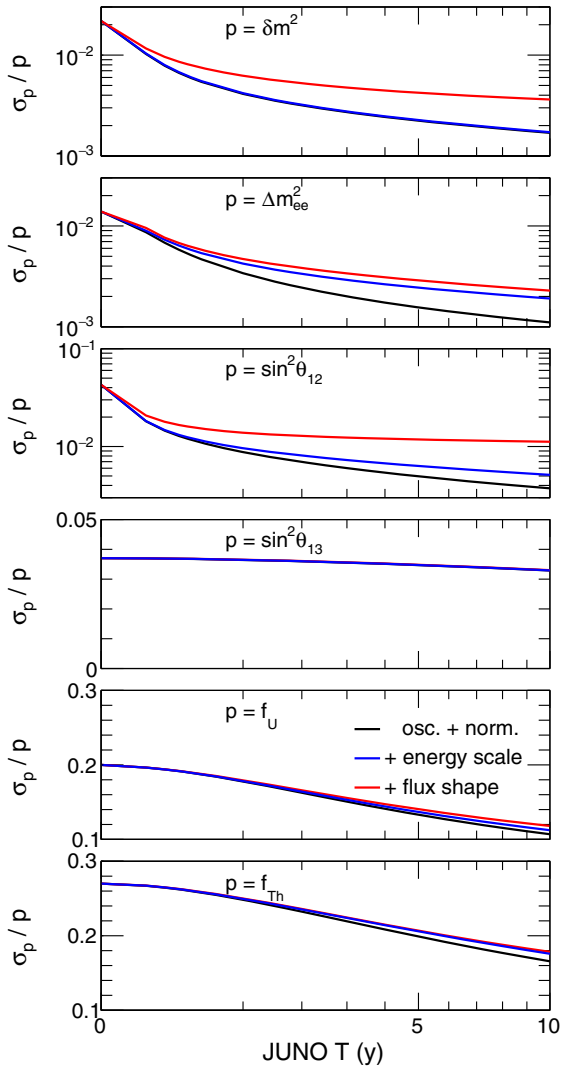

FIG. 10. JUNO analysis: fractional accuracy σ_p/p as a function of live time T for six measurable parameters p. The line color code is the same as in Fig. 8, and the abscissa also scales as $\sqrt{T}$. From top to bottom, the results refer to the squared mass splittings δm^2 and Δm^2_{ee}, the mixing angles $\sin^2\theta_{12}$ and $\sin^2\theta_{13}$, and the geoneutrino flux normalization factors $f_{\rm U}$ and $f_{\rm Th}$. The same results are obtained by using the $S_T \to S_J$ mapping ansatz (not shown).

improved. Finally, we have repeated the analysis by using the $S_T \to S_J$ mapping ansatz, obtaining the same results with insignificant deviations (not shown).

V. NEUTRINO OSCILLOMETRY IN JUNO: ENSEMBLES OF SPECTRA

Summation calculations of reactor spectra have come a long way since the pioneering works [93–96]. Modern realizations are based on thousands of nuclear input data on decay yields Y_i, end points Q_j and branching ratios b_k, together with their uncertainties and possible covariances [57,97]. However, as mentioned in the Introduction, even the most refined summation spectra do not match well current reactor data, suggesting that some nuclear (experimental or theoretical) ingredients may be missing. Significant work is still needed to reach consensus on satisfactory spectra with realistic uncertainties and correlations [61,98], with TAO providing important benchmarks in the future [72].

With all these caveats, we perform an exploratory analysis of the effect of known nuclear input uncertainties on the spectral substructures through the Oklo toolkit [79]. We remind that the Oklo code contains (4306,6609,6804) values for (Y_i, Q_j, b_k), respectively, for a total of $N_d = 17,719$ input data, together with their quoted uncertainties (taken as uncorrelated). These huge numbers prevent usual χ^2 analyses of variant spectra, in terms of marginalization over nuisance parameters. Alternatively, we generate ensembles of N neutrino spectra $\{S^n_\nu(E)\}_{n=1,\ldots,N}$, by randomly varying all or some nuclear inputs within their uncertainties. We also compute the associated TAO spectra $\{S^n_T(E_{\rm vis})\}$, that are then mapped to obtain JUNO spectra $\{S^n_J(E_{\rm vis})\}$ (where we drop the superscript "eff" for simplicity).

We test how these variants affect the JUNO oscillation analysis, and how well they can be distinguished by TAO, by scanning appropriate χ^2 functions over the whole spectral set(s). We recover, through an independent χ^2 analysis, the results obtained in [59] through a Fourier analysis, namely, that known substructure uncertainties do not appear to pose a threat to precision oscillometry in JUNO. However, the quantification of this result is not trivial, and some subtle problems in the statistical analysis will be highlighted. We shall also comment on the issue of possible unknown small-scale uncertainties, as raised, e.g., in [58] and [60,81].

A. Changing all nuclear input uncertainties: Spectrum metric and (under)sampling issues

In our first exercise with spectral variants, we have generated an ensemble of $N = 10^5$ neutrino spectra S^n_ν (and associated TAO spectra S^n_T) by N extractions of random values s^n_i for all the $i = 1, \ldots, N_d$ inputs at the same time, assuming uncorrelated Gaussian distributions for the quoted uncertainties σ_i. At each extraction, branching ratios for each decay are renormalized by an overall factor to ensure unitarity ($\sum_k b_k = 1$). All variant spectra S^n_T are normalized to the same area as the reference spectrum S_T in order to emphasize shape variations.

Figure 11 shows S_T (solid line) with its statistical errors (dark gray band), assuming 3×10^6 IBD events in TAO, and 40 keV bins. Also shown is the envelope of all the S^n_T variant spectra (light gray band) and a few individual variants (very light gray curves). All spectra are divided by the unoscillated JUNO spectrum S_J, analogously to Fig. 3. Since the light gray band is rather large, one may expect

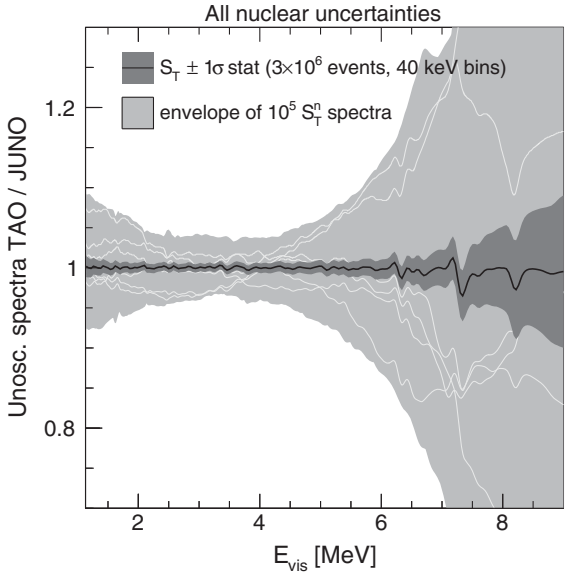

FIG. 11. Spectral ensembles in TAO. Solid line with dark gray band: TAO reference spectrum S_T with its statistical errors, assuming 3×10^6 IBD events and 40 keV bins. Light gray band: envelope of spectra $\{S_T^n\}_{n=1,\ldots,N}$ at TAO, as obtained by $N = 10^5$ extractions of Gaussian-distributed values for all the $N_d = 17$, 719 nuclear input uncertainties in the Oklo toolkit, and normalized to same area as S_T. A few individual variants are also shown (very light gray curves). All spectra are divided by the unoscillated reference JUNO spectrum S_J in order to show fine structures.

that at least some spectral variants within the envelope can play a role in the TAO and JUNO data analyses. The surprising outcome is that only the reference S_T matters in our exercise, for subtle reasons that we could not anticipate.

A first issue is how to define a χ^2_S metric within the $\{S_T^n\}$ envelope, so that 68% (95%) of the spectra fall within a properly defined 1σ (2σ) band etc. (with $N_\sigma = \sqrt{\chi^2_S}$) around the reference spectrum S_T. Note that each spectrum S_T^n is endowed with an χ^2_n value,

$$\chi^2_n = \sum_{i=1}^{N_d} \left(\frac{s_i^n}{\sigma_i}\right)^2, \tag{38}$$

that measures its statistical distance from S_T (having $\chi^2 = 0$ by definition) in terms of nuclear input uncertainties. For $N_d \gg 1$, the distribution of χ^2_n values (not shown) can be approximated by a Gaussian centered at N_d and with variance $2N_d$ [99], effectively starting at 0 (corresponding to S_T) rather than $-\infty$. Since S_T sits in the tail rather than at the peak, this distribution does not directly provide a good metric. However, one can construct a proper metric χ^2_S by integrating this χ^2_n distribution from zero up to the fractional area corresponding to the desired N_σ level. As a result (proof omitted), each spectrum S_T^n is endowed with a new $\chi^2_{S,n}$ value given by

$$\chi^2_{S,n} = 2\left(\mathrm{erf}^{-1}\left(\frac{1}{2} + \frac{1}{2}\mathrm{erf}\left(\frac{\chi^2_n - N_d}{2\sqrt{N_d}}\right)\right)\right)^2, \tag{39}$$

where erf^{-1} is the inverse error function, and $\chi^2_S = 0$ is recovered for S_T in the limit $N_d \gg 1$.

It turns out that if the bands corresponding, e.g., to $\chi^2_{S,n} \leq 1$, 2, and 3 were plotted in Fig. 11, they would be insignificantly smaller than the light gray envelope of all the spectra. In other words, by taking spectra with increasingly high $\chi^2_{S,n}$ (or equivalently χ^2_n), more variant spectral shapes become possible within the band, while the typical substructure amplitudes remain constant and their envelope is not enlarged.

These results suggest caution in parametrizing variant spectra as in [58], namely, by breaking down the envelope in bins and computing uncorrelated standard deviations in each bin, for two reasons: (1) the amplitude of deviations does not scale with N_σ; (2) by binning, the detailed information about which shapes are (not) allowed by nuclear uncertainties is completely lost; in particular, the loss of point-to-point correlations permits more shapes than would be allowed by nuclear inputs only. In doing so, known uncertainties are partly replaced by unknown ones, allowing substructure amplitudes and shapes beyond those pertaining to compiled nuclear inputs.

A second issue concerns the fraction of spectra $\{S_T^n\}$ that survives the comparison with prospective TAO data. We consider a simplified χ^2 analysis for TAO, where each spectrum S_T^n is compared with the reference one S_T in terms of statistical errors, plus one nuisance normalization parameter λ ($S_T^n \to \lambda S_T^n$, assuming $\sigma_\lambda/\lambda = 1.5 \times 10^{-2}$), in addition to $\chi^2_{S,n}$ that embeds nuclear errors,

$$\chi^2_{\mathrm{TAO},n} = \chi^2_{\mathrm{stat},n} + \chi^2_{\mathrm{norm},n} + \chi^2_{S,n}, \tag{40}$$

where for $\chi^2_{\mathrm{stat},n}$ we adopt the limit of infinite bins [77,78,100], that provides a very good approximation to the binned case. Within the ensemble $\{S_T^n\}$, the fraction of spectra allowed at N_σ by TAO data (defined by $\chi^2_{\mathrm{TAO},n} \leq N^2_\sigma$) is a function of the TAO exposure. With $\sim 3 \times 10^6$ IBD events expected in TAO after $\sim$5 years, we unexpectedly find that none of the 10^5 synthetic spectra survives, even at $N_\sigma = 3$ level: they are all rejected with respect to the reference spectrum S_T. It turns out that the good TAO energy resolution is sufficient to distinguish spectra S_T^n that differ from S_T by a few substructures, even with much less than $\sim 3 \times 10^6$ events.

Figure 12 shows how well TAO selects spectra in the ensemble $\{S_T^n\}$, as a function of the total number of collected IBD events. The three curves represent the fraction of spectra that survives at $N_\sigma = 1$, 2, and 3. For no TAO events, these fractions correspond by construction, respectively, to 0.68, 0.95, and 0.997. By increasing the number of TAO events, these fractions drop rapidly.

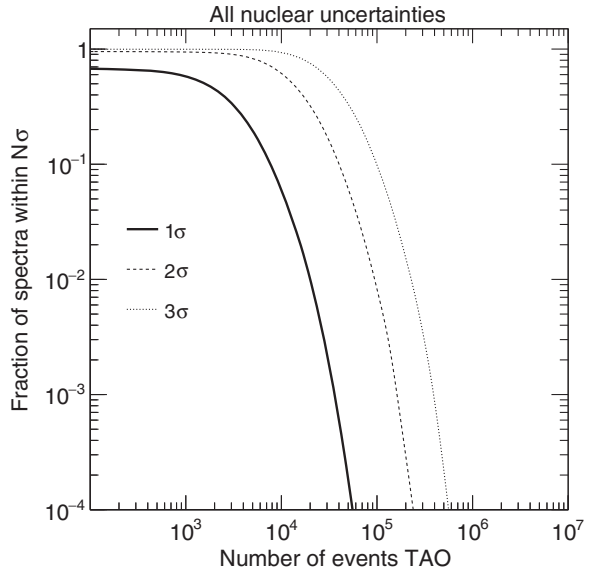

FIG. 12. Spectral ensembles in TAO. Fraction of variant spectra S_T^n (generated by changing all nuclear uncertainties) that survive at N_σ when compared to the reference S_T spectrum, as a function of accumulated TAO events.

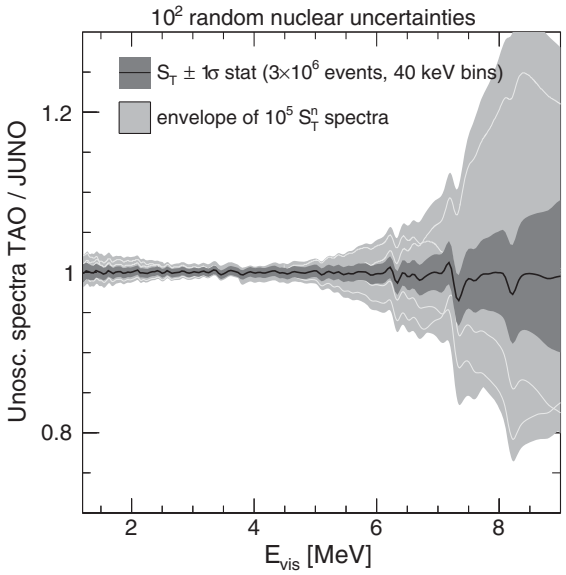

FIG. 13. Spectral ensembles in TAO. As in Fig. 11, but with the light gray band representing the envelope of spectra $\{S_T^n\}_{n=1,\ldots,N}$ at TAO, as obtained by $N = 10^5$ extractions of Gaussian-distributed values for a random set of $N'_d = 10^2$ (out of $N_d = 17,719$) nuclear input uncertainties in the Oklo toolkit.

When the surviving fractions drop below 10^{-4} (not shown), the curves break down because only a handful of the 10^5 spectra—and ultimately none of them—are allowed; this happens well below 3×10^6 events in TAO. The results in Fig. 12 suggest that, when all the nuclear input uncertainties ($N_d = 17,719$) are randomly varied, generating 10^5 synthetic spectra by random extractions is not enough to densely sample the ∞^{N_d}-dimensional set of possible variant spectra: orders of magnitude more extractions would be needed to obtain a few spectra S_T^n really close to S_T within statistical uncertainties.

A third statistical issue, connected with the last one just discussed, concerns the JUNO sensitivity to mass ordering. We have repeated the prospective JUNO data analysis in Sec. IV by mapping the spectral ensemble $\{S_T^n\} \to \{S_J^n\}$ for any set of oscillation parameters. In particular, assuming NO and the reference S_J as the true hypothesis, we have tested the wrong IO not only via S_J but also scanning the 10^5 spectra S_J^n (with and without adding the term $\chi^2_{S,n}$).[6] We have found no reduction of the sensitivity to the mass ordering as compared with Fig. 8.[7] These results qualitatively agree with those in [59] (where a Fourier spectral analysis found that substructures played a little role) but are unexpectedly stronger: none of the test spectra induces any sensitivity reduction in JUNO. In addition, we find that also the precision determination of several parameters p as in Fig. 10 remains unaltered. Once more, we surmise that the ensemble of 10^5 spectra is not dense enough to sample shape variations very close to the reference one. In order to overcome these issues, we construct and test a denser ensemble below.

B. Changing only some nuclear input uncertainties: Suggestions for possible parametrizations

We have constructed an alternative ensemble of 10^5 spectra $\{S_T^n\}$ with substructures closer to the reference spectrum S_T as follows: at each of 10^5 extractions, we have randomly chosen a subset of only $N'_d = 10^2$ nuclear input uncertainties (out of $N_d = 17,719$) to be varied. Figure 13 is analogous to Fig. 11 but shows the envelope of such new spectra, which is narrower and closer to S_T by construction. Also, in this case, by ranking variant spectra with a $\chi^2_{S,n}$ as in Eq. (39) (with N_d replaced by N'_d), the N_σ bands would be only marginally smaller than the envelope, confirming that substructure amplitudes do not scale with N_σ.

Figure 14 is analogous to Fig. 12 but with the new ensemble of spectra. In this case, $O(10^6)$ TAO events are required to start reducing the fractions of spectra allowed at N_σ. For 3×10^6 events, using Eq. (40), we find that the envelope of spectra surviving at 1σ is as shown in Fig. 15. The envelopes at 2σ and 3σ (not shown) are about a factors of 2 and 3 larger than the light gray band in Fig. 15, suggesting that the fit to TAO data tends to linearize the scaling of allowed substructure amplitudes with N_σ.

[6]Our computing resources are saturated for $O(10^5)$ replicas of prospective JUNO data analyses, hence the choice of having no more than 10^5 synthetic spectra.

[7]A similar test with six variant spectra in JUNO (rather than 10^5) was mentioned in [65].

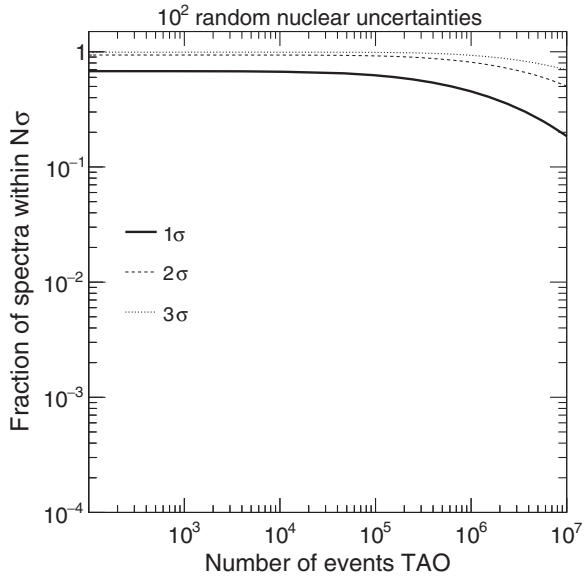

FIG. 14. Spectral ensembles in TAO. As in Fig. 12, but considering only a random subset of 100 nuclear uncertainties.

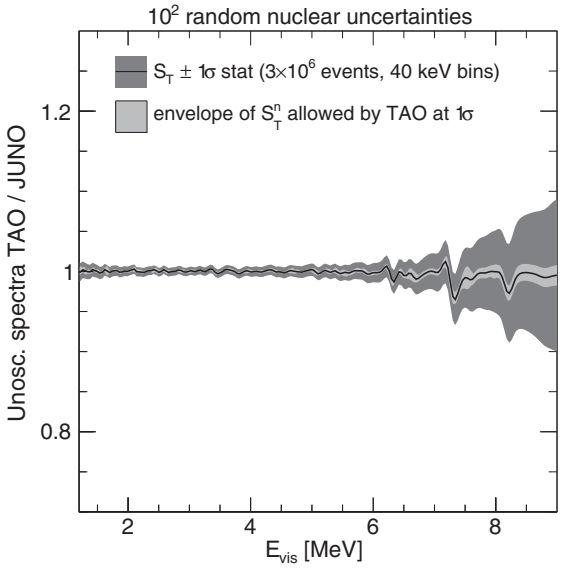

FIG. 15. Spectral ensembles in TAO. As in Fig. 13, but with the light gray band representing the envelope of spectra allowed at 1σ by TAO after collecting 3×10^6 events.

Concerning the JUNO sensitivity to mass ordering, we now find a slight reduction of $\Delta\chi^2(\mathrm{IO}-\mathrm{NO})$, amounting to -0.4 when scanning over the whole new set of $\{S_J^n\}$; this reduction is halved to -0.2 when this set is reduced by TAO via Eq. (40). These relatively small effects, derived through an χ^2 analysis, agree with the Fourier-analysis findings of [59]: variant spectral substructures appear to play a little role in the JUNO sensitivity to mass ordering, as far as known nuclear uncertainties are concerned.[8] The role is even more marginal with the help of TAO. Of course, if all substructures shapes were hypothetically allowed, including oscillatory ones appropriately tuned to "undo" the IO-NO probability differences, then the sensitivity reduction would be higher [58], at the price of introducing *ad hoc* unknown errors, not belonging to those parametrized in nuclear databases.

From the exercises in this subsection and in the previous one, we learn that, once TAO spectral data and an associated reference model spectrum $S_T(E_{\mathrm{vis}})$ will be available, it will be important to sample very densely the functional neighborhood of such spectrum, in order to study the residual effects of allowed variant spectra in JUNO. Brute force variations of all the $O(10^5)$ nuclear decay parameters may lead to undersampling issues in this context. Reduction to a limited number of nuclear error sources appears to be a better strategy. While we have arbitrarily limited this number to 10^2 random error sources, future studies may motivate on more physical grounds a limited subset of nuclear errors (plus possible covariances), related to the decays producing the most pronounced substructures in TAO. If the nuclear physics of reactor neutrino spectra will not be well understood even in the TAO era, these known error sources may be cautiously supplemented (but not replaced) by some extra errors for unknown substructures.

[8]In addition, we find that the fractional precision σ_p/p of the parameters in Fig. 10 remains the same, except for a slight reduction by ∼20% for the Δm^2_{ee} uncertainty. The parameter Δm^2_{ee} governs the frequency of fast oscillations in JUNO and is thus more subject to "noisy" substructure variations.

VI. SUMMARY AND CONCLUSIONS

The next-generation, medium baseline reactor neutrino experiment JUNO (in construction) is planned to probe the full pattern of $\bar{\nu}_e$ disappearance for $L/E \sim (\text{few MeV})/(53\ \text{km})$, including the precision measurements of oscillations induced by the $(\delta m^2, \theta_1 2)$ and $(\Delta m^2, \theta_{13})$ mass-mixing pairs, and their interference effects governed by the neutrino mass ordering, namely, $\mathrm{sign}(\delta m^2/\Delta m^2)$. The supplementary detector TAO is expected to monitor the unoscillated flux close to one reactor core, with about a factor ×2 improvement in energy resolution and with ×30 more events than in JUNO.

In this work, we have studied the relations between the observable event spectra in TAO (S_T) and JUNO (S_J), in the simplifying assumption that they are generated by the same unobservable neutrino spectrum (S_ν), including fine-structure features as emerging in summation calculations. We have used the publicly available Oklo toolkit [79] to generate a reference spectrum S_ν, as well as a number of variants S_ν^n corresponding to changes in the (thousands) of nuclear inputs describing fission yields, branching ratios, and end point energies. Our methodology can be applied to more updated nuclear databases, which are currently being

developed and endowed with preliminary error covariances (not included in this work).

After reviewing in detail the different and non-negligible effects of energy resolution and nucleon recoil on the observable spectra, we have shown that a model spectrum S_T at TAO site can be mapped into a corresponding spectrum S_J at JUNO via well-defined convolutions, without using the (more detailed) information contained in the source neutrino spectrum S_ν. The mapping $S_T \to S_J$ is exact in the hypothetical case of no oscillations, and can be generalized with excellent accuracy to the real case with oscillations, via an ansatz on the effective disappearance probability. The prospective χ^2 analysis of JUNO data confirms the validity of the mapping and allows to discuss the impact of uncertainties related to oscillation parameters, energy-scale and flux-shape systematics.

We have also analyzed the effect of known nuclear input uncertainties, by generating bundles of variant spectra with the Oklo toolkit. We highlight several statistical issues arising from sampling a large number of variable inputs. We find that the bundles must densely sample the neighborhood of the reference spectrum in order to produce a detectable effect on the JUNO χ^2 function in numerical experiments. In this case (realized by sampling only a random subset of nuclear uncertainties), the effect turns out to be small (in agreement with [59]) and can be further reduced by adding TAO constraints. These results, based on known nuclear inputs, also suggest some cautionary comments on parametrizations of unknown substructure uncertainties, in terms of variances of binned bundles.

We have argued that, when TAO data will be available, an optimal strategy to deal with small-scale spectral shape uncertainties will be to focus on a few prominent visible substructures and related nuisance parameters, in order to build a dense ensemble of TAO spectral variants, to be mapped in JUNO and compared with its data. Optimal constructions for such variant ensembles, possibly with covariances of known errors and with allowance for extra unknown errors, as well as for corrections due to different fuel components in the TAO and JUNO sources, are left to future studies. We conclude by observing that, after only two decades from the discovery of neutrino oscillations, the JUNO and TAO projects are bringing the discussion of precision oscillometry to an unprecedented level of details, whose deeper understanding will require further advances at the junction of neutrino and nuclear physics.

ACKNOWLEDGMENTS

We are grateful to Anna Hayes and Alejandro Sonzogni for useful discussions about fine structures in reactor neutrino spectra. We thank Jun Cao, Gioacchino Ranucci, and Monica Sisti for providing us with early information about the TAO project. This work is partly supported by the Italian Ministero dell'Università e Ricerca through the research Grant No. 2017W4HA7S "NAT-NET: Neutrino and Astroparticle Theory Network" under the program PRIN 2017 and by the Istituto Nazionale di Fisica Nucleare through the "Theoretical Astroparticle Physics" (TAsP) project. The work of F. C. is supported by the Deutsche Forschungsgemeinschaft through Grants No. SFB-1258 "Neutrinos and Dark Matter in Astro- and Particle Physics" and No. EXC 2094 "ORIGINS: From the Origin of the Universe to the First Building Blocks of Life."

[1] *History of the Neutrino 1930-2018, Proceedings of the International Conference on History of the Neutrino (Paris, France, 2018)*, edited by M. Cribier, J. Dumarchez, and D. Vignaud (AstroParticle and Cosmology Laboratory (APC), Paris, 2019), http://neutrinohistory2018.in2p3.fr.

[2] S. Bilenky, Prehistory of neutrino oscillation, arXiv:1902.10052, in [1].

[3] C. Jarlskog, Birth of the neutrino, from Pauli to the Reines-Cowan experiment, arXiv:1902.03281, in [1].

[4] P. Vogel, Reactor neutrinos: Toward oscillations, arXiv:1902.03281, in [1].

[5] T. Lasserre, Reactor neutrinos after CHOOZ and KamLAND, in [1].

[6] L. J. Wen, J. Cao, and Y. Wang, Reactor neutrino experiments: Present and future, Annu. Rev. Nucl. Part. Sci. **67**, 183 (2017).

[7] X. Qian and J. Peng, Physics with reactor neutrinos, Rep. Prog. Phys. **82**, 036201 (2019).

[8] V. Antonelli, L. Miramonti, and G. Ranucci, Present and future contributions of reactor experiments to mass ordering and neutrino oscillation studies, Universe **6**, 52 (2020).

[9] A. Gando *et al.* (KamLAND Collaboration), Reactor on-off antineutrino measurement with KamLAND, Phys. Rev. D **88**, 033001 (2013).

[10] D. Adey *et al.* (Daya Bay Collaboration), Measurement of the Electron Antineutrino Oscillation with 1958 Days of Operation at Daya Bay, Phys. Rev. Lett. **121**, 241805 (2018).

[11] G. Bak *et al.* (RENO Collaboration), Measurement of Reactor Antineutrino Oscillation Amplitude and Frequency at RENO, Phys. Rev. Lett. **121**, 201801 (2018).

[12] H. de Kerret *et al.* (Double Chooz Collaboration), First double Chooz θ_{13} measurement via total neutron capture detection, Nat. Phys. **16**, 558 (2020).

[13] M. C. Gonzalez-Garcia and M. Yokoyama, Review on neutrino masses, mixing and oscillations, in P. A. Zyla

et al. (Particle Data Group), Prog. Theor. Exp. Phys. **2020**, 083C01 (2020), http://pdg.lbl.gov.
[14] S. Petcov and M. Piai, The LMA MSW solution of the solar neutrino problem, inverted neutrino mass hierarchy and reactor neutrino experiments, Phys. Lett. B **533**, 94 (2002).
[15] Y. F. Li, J. Cao, Y. Wang, and L. Zhan, Unambiguous determination of the neutrino mass hierarchy using reactor neutrinos, Phys. Rev. D **88**, 013008 (2013).
[16] F. An *et al.* (JUNO Collaboration), Neutrino physics with JUNO, J. Phys. G **43**, 030401 (2016).
[17] A. Hayes and P. Vogel, Reactor neutrino spectra, Annu. Rev. Nucl. Part. Sci. **66**, 219 (2016).
[18] P. Huber, Reactor antineutrino fluxes status and challenges, Nucl. Phys. **B908**, 268 (2016).
[19] M. Dentler, A. Hernández-Cabezudo, J. Kopp, M. Maltoni, and T. Schwetz, Sterile neutrinos or flux uncertainties? Status of the reactor anti-neutrino anomaly, J. High Energy Phys. 11 (2017) 099.
[20] C. Giunti, Y. Li, B. Littlejohn, and P. Surukuchi, Diagnosing the reactor antineutrino anomaly with global antineutrino flux data, Phys. Rev. D **99**, 073005 (2019).
[21] J. M. Berryman and P. Huber, Sterile neutrinos and the global reactor antineutrino dataset, arXiv:2005.01756.
[22] Y. Ko *et al.* (NEOS Collaboration), Sterile Neutrino Search at the NEOS Experiment, Phys. Rev. Lett. **118**, 121802 (2017).
[23] V. Zacek, G. Zacek, P. Vogel, and J. Vuilleumier, Evidence for a 5 MeV spectral deviation in the goesgen reactor neutrino oscillation experiment, arXiv:1807.01810.
[24] P. Huber, NEOS Data and the Origin of the 5 MeV Bump in the Reactor Antineutrino Spectrum, Phys. Rev. Lett. **118**, 042502 (2017).
[25] Y. Gebre, B. Littlejohn, and P. Surukuchi, Prospects for improved understanding of isotopic reactor antineutrino fluxes, Phys. Rev. D **97**, 013003 (2018).
[26] C. Giunti, Improved determination of the ^{235}U and ^{239}Pu reactor antineutrino cross sections per fission, Phys. Rev. D **96**, 033005 (2017).
[27] A. C. Hayes, G. Jungman, E. McCutchan, A. A. Sonzogni, G. T. Garvey, and X. Wang, Analysis of the Daya Bay Reactor Antineutrino Flux Changes with Fuel Burnup, Phys. Rev. Lett. **120**, 022503 (2018).
[28] D. Adey *et al.* (Daya Bay Collaboration), Improved measurement of the reactor antineutrino flux at Daya Bay, Phys. Rev. D **100**, 052004 (2019).
[29] D. Adey *et al.* (Daya Bay Collaboration), Extraction of the ^{235}U and ^{239}Pu Antineutrino Spectra at Daya Bay, Phys. Rev. Lett. **123**, 111801 (2019).
[30] G. Bak *et al.* (RENO Collaboration), Fuel-Composition Dependent Reactor Antineutrino Yield at RENO, Phys. Rev. Lett. **122**, 232501 (2019).
[31] J. Ashenfelter *et al.* (PROSPECT Collaboration), Measurement of the Antineutrino Spectrum from ^{235}U Fission at HFIR with PROSPECT, Phys. Rev. Lett. **122**, 251801 (2019).
[32] A. Hayes, J. Friar, G. Garvey, D. Ibeling, G. Jungman, T. Kawano, and R. W. Mills, Possible origins and implications of the shoulder in reactor neutrino spectra, Phys. Rev. D **92**, 033015 (2015).
[33] A. A. Sonzogni, E. A. McCutchan, T. D. Johnson, and P. Dimitriou, Effects of Fission Yield Data in the Calculation of Antineutrino Spectra for U235(n,fission) at Thermal and Fast Neutron Energies, Phys. Rev. Lett. **116**, 132502 (2016).
[34] A. Sonzogni, E. McCutchan, and A. Hayes, Dissecting Reactor Antineutrino Flux Calculations, Phys. Rev. Lett. **119**, 112501 (2017).
[35] X. Ma, L. Yang, L. Zhan, F. An, and J. Cao, Investigation of antineutrino spectral anomaly with updated nuclear database, arXiv:1807.09265.
[36] G. Mention, M. Vivier, J. Gaffiot, T. Lasserre, A. Letourneau, and T. Materna, Reactor antineutrino shoulder explained by energy scale nonlinearities? Phys. Lett. B **773**, 307 (2017).
[37] J. Hardy, L. Carraz, B. Jonson, and P. Hansen, The essential decay of pandemonium: A demonstration of errors in complex beta-decay schemes, Phys. Lett. **71B**, 307 (1977).
[38] M. Fallot *et al.*, New Antineutrino Energy Spectra Predictions from the Summation of Beta Decay Branches of the Fission Products, Phys. Rev. Lett. **109**, 202504 (2012).
[39] B. Rasco *et al.*, Decays of the Three Top Contributors to the Reactor $\bar{\nu}_e$ High-Energy Spectrum, ^{92}Rb, ^{96gs}Y, and ^{142}Cs, Studied with Total Absorption Spectroscopy, Phys. Rev. Lett. **117**, 092501 (2016).
[40] V. Guadilla *et al.*, Total absorption γ-ray spectroscopy of the β-delayed neutron emitters ^{137}I and ^{95}Rb, Phys. Rev. C **100**, 044305 (2019).
[41] V. Guadilla *et al.*, Total absorption γ-ray spectroscopy of niobium isomers, Phys. Rev. C **100**, 024311 (2019).
[42] V. Guadilla *et al.*, Large Impact of the Decay of Niobium Isomers on the Reactor $\bar{\nu}_e$ Summation Calculations, Phys. Rev. Lett. **122**, 042502 (2019).
[43] M. Estienne *et al.*, Updated Summation Model: An Improved Agreement with the Daya Bay Antineutrino Fluxes, Phys. Rev. Lett. **123**, 022502 (2019).
[44] V. Guadilla *et al.*, Determination of beta decay ground state feeding of nuclei of importance for reactor applications, arXiv:2005.08780.
[45] A. Hayes, J. Friar, G. Garvey, G. Jungman, and G. Jonkmans, Systematic Uncertainties in the Analysis of the Reactor Neutrino Anomaly, Phys. Rev. Lett. **112**, 202501 (2014).
[46] X. Wang and A. Hayes, Weak magnetism correction to allowed β decay for reactor antineutrino spectra, Phys. Rev. C **95**, 064313 (2017).
[47] Y. Li and D. Zhang, New realization of the conversion calculation for reactor antineutrino fluxes, Phys. Rev. D **100**, 053005 (2019).
[48] D. L. Fang and B. Brown, Effect of first forbidden decays on the shape of neutrino spectra, Phys. Rev. C **91**, 025503 (2015).
[49] D. Fang, Y. Li, and D. Zhang, *Ab initio* calculations of reactor antineutrino fluxes with exact lepton wave functions, arXiv:2001.01689.
[50] T. Yoshida, T. Tachibana, S. Okumura, and S. Chiba, Spectral anomaly of reactor antineutrinos based on theoretical energy spectra, Phys. Rev. C **98**, 041303 (2018).

[51] J. Petković, T. Marketin, G. Martínez-Pinedo, and N. Paar, Self-consistent calculation of the reactor antineutrino spectra including forbidden transitions, J. Phys. G **46**, 085103 (2019).
[52] L. Hayen, J. Kostensalo, N. Severijns, and J. Suhonen, First forbidden transitions in the reactor anomaly, Phys. Rev. C **100**, 054323 (2019).
[53] L. Hayen, J. Kostensalo, N. Severijns, and J. Suhonen, First-forbidden transitions in reactor antineutrino spectra, Phys. Rev. C **99**, 031301 (2019).
[54] P. Vogel, Conversion of electron spectrum associated with fission into the antineutrino spectrum, Phys. Rev. C **76**, 025504 (2007).
[55] D. Dwyer and T. Langford, Spectral Structure of Electron Antineutrinos from Nuclear Reactors, Phys. Rev. Lett. **114**, 012502 (2015).
[56] A. Sonzogni, T. Johnson, and E. McCutchan, Nuclear structure insights into reactor antineutrino spectra, Phys. Rev. C **91**, 011301 (2015).
[57] A. Sonzogni, M. Nino, and E. McCutchan, Revealing fine structure in the antineutrino spectra from a nuclear reactor, Phys. Rev. C **98**, 014323 (2018).
[58] D. V. Forero, R. Hawkins, and P. Huber, The benefits of a near detector for JUNO, arXiv:1710.07378.
[59] D. Danielson, A. Hayes, and G. Garvey, Reactor neutrino spectral distortions play little role in mass hierarchy experiments, Phys. Rev. D **99**, 036001 (2019).
[60] Z. Cheng, N. Raper, W. Wang, C. F. Wong, and J. Zhang, Potential impact of sub-structure on the resolution of neutrino mass hierarchy at medium-baseline reactor neutrino oscillation experiments, arXiv:2004.11659.
[61] Technical Meeting on Nuclear Data for Anti-neutrino Spectra and Their Applications, IAEA, Vienna, 2019, Contributions available at the website, https://www-nds.iaea.org/index-meeting-crp/Antineutrinos.
[62] L. Mikaelyan and V. Sinev, Searches for sterile neutrinos at reactor, Phys. At. Nucl. **62**, 2008 (1999).
[63] L. Mikaelyan and V. Sinev, Neutrino oscillations at reactors: What next? Phys. At. Nucl. **63**, 1002 (2000).
[64] Y. Wang (JUNO Collaboration), Unknowns of neutrinos, in the final discussion on perspectives in neutrino and multi messenger physics, in *NEUTEL 2017, XVII International Workshop on Neutrino Telescopes (Venice, Italy, 2017)* (2017), https://agenda.infn.it/event/11857.
[65] L. Zhan (JUNO Collaboration), A high energy resolution detector for the measurement of reactor antineutrino spectrum, in *ESCAPE 2018, Workshop on Energy Scale Calibration in Antineutrino Precision Experiments, Heidelberg, Germany, 2018* (2018), https://www.mpi-hd.mpg.de/escape2018, https://dx.doi.org/10.5281/zenodo.1314423.
[66] B. Wonsak (JUNO Collaboration), Status and prospects of the JUNO experiment, in *Neutrino 2018, XXVIII International Conference on Neutrino Physics and Astrophysics, Heidelberg, Germany, 2018* (2018), https://www.mpi-hd.mpg.de/nu2018, https://dx.doi.org/doi:10.5281/zenodo.1286850.
[67] J. Cao (JUNO Collaboration), Measuring high resolution reactor neutrino spectrum with JUNO-TAO, talk at [61]; reactor neutrino anomalies, in *19th Lomonosov Conference on Elementary Particle Physics, Moscow, Russia, 2019* (2019), http://lomcon.ru/?page_id=204.
[68] G. Ranucci (JUNO Collaboration), JUNO oscillation physics program, Proc. Sci., NOW2018 (**2018**) 024.
[69] W. Wang (JUNO) Collaboration, Taishan antineutrino observatory, in *NNN 2019, 20th International Workshop on Next Generation Nucleon Decay and Neutrino Detectors, Medellin, Colombia, 2019* (2019), https://indico.cern.ch/event/835190.
[70] M. Sisti (JUNO Collaboration), Physics prospects of the JUNO experiment, J. Phys. Conf. Ser. **1468**, 012150 (2020).
[71] M. V. Smirnov (JUNO), Status and physics of the JUNO experiment, in *Seminar at the High Energy Physics Division of the Petersburg Nuclear Physics Institute* (PNPI, Saint-Petersburg, Russia, 2020), http://hepd.pnpi.spb.ru/hepd/events/seminar_index.html.
[72] A. Abusleme *et al.* (JUNO Collaboration), TAO conceptual design report: A precision measurement of the reactor antineutrino spectrum with sub-percent energy resolution, arXiv:2005.08745.
[73] D. Brown *et al.*, ENDF/B-VIII.0: The 8th major release of the nuclear reaction data library with CIELO-project cross sections, new standards and thermal scattering data, Nucl. Data Sheets **148**, 1 (2018).
[74] K. Schmidt and B. Jurado, Review on the progress in nuclear fission–experimental methods and theoretical descriptions, Rep. Prog. Phys. **81**, 106301 (2018).
[75] L. A. Bernstein, D. A. Brown, A. J. Koning, B. T. Rearden, C. E. Romano, A. A. Sonzogni, A. S. Voyles, and W. Younes, Our future nuclear data needs, Annu. Rev. Nucl. Part. Sci. **69**, 109 (2019).
[76] H. Ejiri, J. Suhonen, and K. Zuber, Neutrino-nuclear responses for astro-neutrinos, single beta decays and double beta decays, Phys. Rep. **797**, 1 (2019).
[77] F. Capozzi, E. Lisi, and A. Marrone, Neutrino mass hierarchy and electron neutrino oscillation parameters with one hundred thousand reactor events, Phys. Rev. D **89**, 013001 (2014).
[78] F. Capozzi, E. Lisi, and A. Marrone, Neutrino mass hierarchy and precision physics with medium-baseline reactors: Impact of energy-scale and flux-shape uncertainties, Phys. Rev. D **92**, 093011 (2015).
[79] D. Dwyer, OKLO: A toolkit for modeling nuclides and nuclear reactions, https://github.com/dadwyer/oklo (2015).
[80] B. Littlejohn, A. Conant, D. Dwyer, A. Erickson, I. Gustafson, and K. Hermanek, Impact of fission neutron energies on reactor antineutrino spectra, Phys. Rev. D **97**, 073007 (2018).
[81] E. Ciuffoli, J. Evslin, and H. Mohammed, Uncertainty in the reactor neutrino spectrum and mass hierarchy determination, J. High Energy Phys. 10 (2019) 143.
[82] P. Vogel and J. F. Beacom, Angular distribution of neutron inverse beta decay, $\bar{\nu}_e + p \to e^+ + n$, Phys. Rev. D **60**, 053003 (1999).
[83] A. Strumia and F. Vissani, Precise quasielastic neutrino/nucleon cross-section, Phys. Lett. B **564**, 42 (2003).
[84] F. Vissani, Comparative analysis of SN1987A antineutrino fluence, J. Phys. G **42**, 013001 (2015).

[85] L. Wei, L. Zhan, J. Cao, and W. Wang, Improving the energy resolution of the reactor antineutrino energy reconstruction with positron direction, arXiv:2005.05034.
[86] Y. F. Li, Y. Wang, and Z. z. Xing, Terrestrial matter effects on reactor antineutrino oscillations at JUNO or RENO-50: How small is small?, Chin. Phys. C **40**, 091001 (2016).
[87] A. N. Khan, H. Nunokawa, and S. J. Parke, Why matter effects matter for JUNO, Phys. Lett. B **803**, 135354 (2020).
[88] H. Minakata, H. Nunokawa, S. J. Parke, and R. Zukanovich Funchal, Determination of the neutrino mass hierarchy via the phase of the disappearance oscillation probability with a monochromatic $\bar{\nu}_e$ source, Phys. Rev. D **76**, 053004 (2007).
[89] F. Capozzi, E. Lisi, A. Marrone, and A. Palazzo, Current unknowns in the three neutrino framework, Prog. Part. Nucl. Phys. **102**, 48 (2018).
[90] S. Parke, What is Δm^2_{ee}? Phys. Rev. D **93**, 053008 (2016).
[91] X. Qian, D. Dwyer, R. McKeown, P. Vogel, W. Wang, and C. Zhang, Mass hierarchy resolution in reactor anti-neutrino experiments: Parameter degeneracies and detector energy response, Phys. Rev. D **87**, 033005 (2013).
[92] D. Adey *et al.* (Daya Bay Collaboration), A high precision calibration of the nonlinear energy response at Daya Bay, Nucl. Instrum. Methods Phys. Res., Sect. A **940**, 230 (2019).
[93] R. King and J. Perkins, Inverse beta decay and the two-component neutrino, Phys. Rev. **112**, 963 (1958).
[94] F. T. Avignone, S. M. Blakenship, and C. W. Darden, Theoretical fission-antineutrino spectrum and cross section of the reaction ^{3}He$(\bar{\nu}_e, e^+)^3$H, Phys. Rev. **170**, 931 (1968).
[95] B. Davis, P. Vogel, F. Mann, and R. Schenter, Reactor anti-neutrino spectra and their application to anti-neutrino induced reactions, Phys. Rev. C **19**, 2259 (1979).
[96] F. Avignone III and C. Greenwood, Calculated spectra of antineutrinos from U-235, U-238, and Pu-239, and anti-neutrino-induced reactions, Phys. Rev. C **22**, 594 (1980).
[97] A. Sonzogni, Uncertainty quantification in the summation method for nuclear reactor antineutrinos, talk at [61].
[98] A. Sonzogni, Development of realistic uncertainties in the summation method for nuclear reactor antineutrino applications, talk at *AAP 2019, Workshop on Applied Anti-neutrino Physics, Sun Yat-sen, China, 2019* (2019), https://indico.cern.ch/event/833568.
[99] G. Cowan, Review on probability, in P. A. Zyla *et al.* (Particle Data Group), Prog. Theor. Exp. Phys. **2020**, 083C01 (2020), http://pdg.lbl.gov.
[100] S. F. Ge, K. Hagiwara, N. Okamura, and Y. Takaesu, Determination of mass hierarchy with medium baseline reactor neutrino experiments, J. High Energy Phys. 05 (2013) 131.